SEMI-ANNUAL PROGRESS REPORT

FOR CONTRACT NASW-4814

CORONAL ABUNDANCES AND THEIR VARIATION

Date: 15 December 1994

Principal Investigator and Author:

Julia L.R. Saba (Lockheed Organization 91-3H)

Author's address (Lockheed Remote Site):

Code 682.2, NASA/Goddard Space Flight Center
Greenbelt, Maryland 20771

Institution address:

Lockheed Palo Alto Research Laboratory
Organization 91-30, Building 252
3251 Hanover Street
Palo Alto, California 93404

ABSTRACT

This contract supports the investigation of elemental abundances in the solar corona, principally through analysis of high-resolution soft X-ray spectra from the Flat Crystal Spectrometer on NASA's Solar Maximum Mission. The goals of the study are a characterization of the mean values of relative abundances of elements accessible in the FCS data, and information on the extent and circumstances of their variability. This report is a summation of the data analysis and reporting activities which occurred since the last report, submitted two months early, in April 1994, to facilitate evaluation of the first year's progress for contract renewal. Hence this report covers the period 15 April 1994 - 15 December 1994.

Subject terms: Solar corona, X-ray spectra, elemental abundances, abundance variability

CORONAL ABUNDANCES AND THEIR VARIATION

I. INTRODUCTION

This is a semi-annual progress report for contract NASW-4814. The contract resulted from an award under NASA's Supporting Research & Technology Program. Funding of a three-year contract began in June 1993. The contract was renewed for a second year in June 1994. The contract provides funding for the PI at about half-time effort. Since the last report was submitted two months early, in April 1994 rather than June 1994, to permit timely evaluation of progress and continuation of funding, this report covers an eight-month period, namely 15 April - 15 December 1994, rather than the nominal six-month period. Still, not as much was performed on this contract during this reporting period as originally planned, since the PI was heavily engaged in writing proposals over the summer and then in refereeing proposals (neither of which activity was charged to this contract).

However, there were several significant accomplishments during the period, including a talk given at the joint American Geophysical Union/Solar Physics Division meeting in Baltimore in May, and an invited review at COSPAR meeting in Hamburg, for which a refereed paper is now in press in Advances in Space Research. Preparation for these talks and the feedback received at the meetings helped to clarify some ideas on several important issues involved in the contract research. Further, on the way to the COSPAR meeting in Hamburg, the PI visited the Service d'Atrophysique, Centre d'etudes de Saclay near Paris on her way to the COSPAR meeting in Hamburg and had some very useful discussions with Dr. Jean-Paul Meyer and Dr. Monique Arnaud on a variety of topics directly related to the research. (Saclay underwrote the costs for this portion of the foreign travel.)

Also during this period, the PI has been working with colleagues Dr. Joan Schmelz (Rhodes College, Memphis, Tennessee) and Dr. Keith Strong (Lockheed, Palo Alto, California) on the draft of a paper which examines anomalous neon abundances in nonflaring active regions using a combination of two analysis techniques, as discussed below in §III.D.)

II. SCIENTIFIC BACKGROUND

The contract supports an investigation of elemental abundances in the outer atmosphere of the Sun, principally through analysis of high-resolution soft X-ray spectra from the Flat Crystal Spectrometer (FCS) on the *Solar Maximum Mission (SMM)*, a NASA mission dedicated to solar observations from 1980 through 1989. This instrument acquired an excellent data base for studying the relative amounts of oxygen, neon, magnesium, and iron in solar active regions in various states of evolution and activity. The project includes analysis of this data base to decouple the effects of temperature and abundance, to assess different theoretical calculations of spectral line intensities for use in the study, and to account for the possible effects of opacity due to resonance scattering of certain bright lines. The goals of the study are a characterization of the mean values of relative abundances of elements accessible in the FCS data, information on the extent of their variability, identification of possible correlations of variability with active region properties, and clarification of a possible association between abundance variability and active region dynamics.

Much of the observed variation in abundances between the photosphere and the corona appears to be associated with the first ionization potential (FIP) of the elements: elements with low FIP are systematically enhanced in the corona, solar wind, and solar energetic particles (SEP) relative to high-FIP elements, as compared with the photospheric composition. Although there is no convincing detailed quantitative model yet available, theoretical work in this area appears to be progressing, according to a review talk given by Jean-Claude Henoux at the COSPAR meeting in Hamburg. The basic idea is that some element separation mechanism operates in a temperature regime of about 10,000 K where low-FIP elements are ionized while high-FIP elements remain neutral. However, spectroscopic data from *SMM* and other spaceraft show that coronal abundances in closed coronal structures present a more complex story than a simple two-step distribution of abundances (of high- vs. low-FIP elements) relative to photospheric values seen in the slow solar wind and in SEP events. There is also disagreement between the spectroscopic and particle measurements of the normalization of abundances relative to hydrogen, and in fact some disagreement among the different spectroscopic measurements. Knowing the abundances relative to hydrogen is crucial for many aspects of solar spectral data interpretation, beginning with converting line intensities to emission measure (i.e., the amount of emitting material). An attempt to reconcile some of the different spectroscopic measurements was made in the invited review of coronal spectroscopic results given by the PI in Hamburg in July 1994 (see §IV and attached preprint).

Previous work by us (e.g., Strong et al. 1991, Saba & Strong 1993) and by others (e.g., McKenzie and Feldman 1992) has showed that ratios of low-FIP to high-FIP elements appear to vary at least about a factor of four, approximately from the photospheric values to the nominal coronal values defined by the SEP results. The precise upper and lower boundary values depend on the theoretical line emissivity calculations used for both the abundance line ratios and the temperature diagnostics. The question of the shortest observed timescale for variability hinges on the correctness of the line emissivity calculations as well, since the predicted emissivities are used to untangle changes in the abundance from evolution in the temperature. A key component in the predicted emissivity is the ionization fraction, i.e., how much of the element as a function of temperature is in the correct stage of ionization to emit the observed line; under typical "coronal conditions" of low density and local thermodynamic equilbrium, the ionization fraction is a factor which multiplies the effective probability of transition between the electron levels corresponding to the energy of the observed line.

III. CURRENT PROGRESS

During the reporting period, 15 April to 15 December 1994, the PI has made progress in the following areas:

(a) understanding better the issues and uncertainties in the ionization balance calculations used for the abundance analysis,
(b) quantifying the role of resonance scattering in the measured line intensities,
(c) examining measurements of absolute elemental abundances (i.e., abundances normalized relative to hydrogen), and
(d) exploring anomalous neon abundances in active regions.

These are each discussed in more detail below.

A. Ionization Balance

The PI took advantage of her visit to Saclay to discuss at length with Dr. Monique Arnaud the uncertainties involved in ionization balance calculations in general, and in particular in the new calculations for iron by Arnaud & Raymond (199x) [hereafter, ARA]. In some cases, the new calculations give significantly different results from previous calculations by Arnaud & Rothenflug (1985) [hereafter, ARO], and predict very different temperature behaviour for Fe XVII/Ne IX in the regime of 2-5 MK. The ARO calculations predict that this line ratio should be very flat over the temperature regime relevant for active regions, while the ARA calculations predict an increase with temperature, so that the deconvolution of derived abundance and temperature are substantially different. In comparisons with data from the *SMM* FCS, the new ARA calculations appear less consistent than the older ARO calculations for Fe XVII and Fe XVIII in the regime of a few MK. In particular, they imply that most of the time the relative Fe/Ne abundances in the FCS coronal measurements are less than the photospheric value, which would be very troubling. This would mean that the FIP-based picture is not even approximately right for spectroscopic measurements of closed coronal structured. However, it remains to be seen whether the apparent difficulties with the ARA calculations are in fact due instead to effects of resonant scattering or inadequate calculations for the Fe XVII or Fe XVIII excitation rates. It should be noted that, while the two calculations give different boundaries for the range of Fe/Ne variability, the overall magnitude of the variability is comparable; also, while the ARA calculations imply that the variations on timescales less than an hour are due to temperature evolution rather than a change in abundance, day-to-day changes in the active region abundances remain. After discussions with Dr. Arnaud at Saclay, the PI has tentatively concluded that the best calculations would probably lie in between the ARA and ARO results for the cases relevant for the FCS analysis, so that these two extremes can be used to bound the uncertainties. The ionization balance calculations for may other abundant elements are currently being reconsidered by a community of theoreticians in preparation for SoHO analyses (H. Mason, priv. comm. at COSPAR meeting).

B. Resonance Scattering Effects

The recent paper by Waljeski et al. (1994) finds that the magnitude of the resonance scattering effect in active regions may be even larger for certain bright X-ray lines than had been found by Schmelz, Saba, and Strong (1992). Schmelz et al. suggested that the apparent depletion in the flux of the bright Fe XVII line at 15.01 Å, a factor of two to three below predicted theoretical values compared to other bright resonance lines, might be due to resonance scattering. (This effect was discussed in detail in the last progress report.) The Fe XVII line at 15.01Å featured importantly in the early FCS abundance analysis. Waljeski et al. argue that it is insufficient to omit this one line from the analysis, since the effect of resonant scattering on other lines used could also be significant.

The new analysis by Waljeski et al. has the advantage of having considered two Fe XVII lines to estimate the importance of resonance scattering, the the 15.01Å line and a line at 16.78Å which has about 25% of the opacity of the 15.01Å line, and so it avoids possible

effects from uncertain relative abundances of different species. However, the estimated uncertainties of the predicted emissivities for the two Fe XVII line (A. Bhatia, priv. comm.) produce a large uncertainty in their expected line ratio, which in turn yields a large uncertainty in the derived opacity of the 15.01Å line, which is comparable to the difference between the two sets of results. When the PI analyzed additional data from the same active region, using another Fe XVII line which is essentially unaffected by resonance scattering, the magnitude of the effect was found to be closer to the original Schmelz et al. result rather than the newer Waljeski et al. result, even though in principal the latter was done more self-consistently than the former. That is, the optical depths for the Fe XVII line at 15.01 Å appear to be closer to 2 than to 4, and the other lines used are essentially unaffected within the uncertainties. This interim result was reported at the AGU/SPD meeting in Baltimore in May, and will be incorporated in a paper being outlined which will compare the Fe XVII calculations with the FCS observationbs.

Assessment of the magnitude of the effect of resonance scattering in the FCS data and the impact on the derived abundance variability continues. In the coming months, we will resume our comparison of the various theoretical calculations available for five bright Fe XVII lines covered by the FCS spectra and consult with several theoreticians who have performed some of the relavant calculations. Several theoreticians attending the COSPAR session on abundances (private comm. from A.H. Gabriel and F. Bely-Dubau) believe that the whole set of Fe XVII calculations should be revisited, to look for a basic problem with the calculation of the intensity of the 15.01Å line that is unrelated to resonance scattering or other transport effects. In the mean time, the abundance analysis is being continued using the Fe XVII line at 16.78 Å which can be treated as optically thin to scatter.

C. Absolute Elemental Abundances

In the last few months, as a result of further thought and discussion, the PI has come to realize that, even if it is confirmed that resonance scattering is the sole source of the discrepancy between measured and predicted fluxes for the Fe XVII line at 15.01Å, there are two problems with attempting to exploit resonance scattering to try to normalize abundances relative to hydrogen, as was attempted by Waljeski et al.: (i) the resonance scattering process in the active region geometry needs to be modeled more exactly to derive the calculated opacity to an accuracy better than about a factor of two; and (ii) the required substitution of the volume emission measure term for the integrated column density neglects a geometric term which is roughly proportional to $L \times f_L/F_A$, where f_L and F_A are the volume and area filling factors, respectively. Thus the net systematic uncertainty could easily be comparable in magnitude to the typical low-FIP/high-FIP enhancement factor in the corona. These difficulties may be overcome with future observations which combine direct information on the appropriate geometric model (from high-resolution imaging) and independent information on the electron density, from a density-diagnostic line ratio which must be appropriate for the temperature regime of formation of the resonantly scattered line.

Other methods of obtaining absolute abundances from spectroscopic measurements, and some attempts to reconcile the different results, were discussed in the COSPAR review paper and are noted in the accompanying preprint. In brief, in some cases it appears that

line-to-continuum flare abundance studies may have considered plasmas at temperatures sufficiently low that the free-bound component of the continuum was important, without using a self-consistent treatment of the elements contributing to the continuum. Some of the discrepancies between the *SMM* Bent Crystal Spectrometer and the *Yohkoh* Bragg Crystal Spectrometer abundance results may turn out to be related to differences in the two instruments. In particular, the *Yohkoh* BCS has a full-Sun field of view which may allow contamination of the "flare continuum" by cooler solar flux from regions not involved in the flare (J.L. Culhane, public comment during discussion at the COSPAR meeting). This would effectively reduce the derived abundances, which is consistent with the direction of the systematic *SMM* and *Yohkoh* discrepancy, although careful work by the *Yohkoh* BCS team members (many of whom were also involved in *SMM* abundance studies) is required to sort this out definitively.

D. Neon Abundance Anomalies in Active Regions

As discussed in the last report, two complementary methods of abundance analysis are now being combined to improve the FCS active region abundance study. The line-ratio analysis, which yields pair-wise relative abundances provided the emitting plasma is isothermal (or the emissivity functions have identical shapes in the relevant regime), is being used in parallel with a method which overlays curves of the line emissivities as a function of temperature. The different curves should overlap in a single temperature/emission measure solution if the plasma is indeed isothermal and the correct relative abundances are used or if reasonable adjustments to them can be made by simply shifting the curves vertically. An example of this second approach is shown in Figure 2 from the attached preprint of the COSPAR review paper. (The left panel shows nonintersecting curves for multithermal plasma during a flare; the right panel shows nearly isothermal plasma during the flare decay.)

The advantages of combining this method with the current analysis are (i) that it provides a result that is less sensitive to any specific temperature diagnostic and (ii) that it makes it easier to keep track of the joint relative abundances of the four elements O, Ne, Mg, and Fe, without having to explicitly divide out the temperature dependences. In turn, this will guide the deconvolution of temperature and abundance effects which is the goal of the line-ratio analysis.

As noted in the introduction section, the PI is now working with Drs. Schmelz and Strong to apply these combined methods to search for and confirm neon abundance anomalies in nonflaring active regions. A paper is being drafted which discusses the detection of anomalous neon abundances (with ratios of neon to oxygen both higher and lower than expected for photospheric values). Although the bulk of the FCS spectra show the expected ratios, within the statistic and systematic uncertainties, the occurrennce of anomalous abundances for the high-FIP neon, particularly in observations of quiescent active regions, are troubling for the commonly invoked FIP-based models of coronal composition. This anomalous variability shows that a competing element differentiation mechanism or mechanisms must apply.

IV. PUBLICATIONS AND PRESENTATIONS

During the reporting period, the following presentations were made under this contract:

A talk at the joint American Geophysical Union–American Astronomical Society/ Solar Physics Division Meeting in Baltimore, Maryland, in May 1994 was given on *A Reexamination of the Impact of Resonance Scattering on FCS Active Region Abundance Measurements.*

An invited review on the subject *Spectroscopic Measurements of Element Abundances in the Solar Corona: Variations on the FIP Theme* was given at the 30th Assembly of the Committee on Space Research (COSPAR) held in Hamburg, Germany in July 1994, in a special one-day session on *Element Abundance Variations in the Sun and the Heliosphere.* A review paper summarizing the key points of the talk was submitted, refereed, and accepted for publication in Advances in Space Research, and a camera-ready manuscript was prepared. A preprint is attached.

During this reporting period, two papers were published involving work done under the first year of the contract:

The Composition of a Coronal Active Region, by K. Waljeski, D. Moses, K.P. Dere, J.L.R. Saba, K.T. Strong, D.F. Webb, and D.M. Zarro, appeared in the Astrophysical Journal in July 1994. A photocopy of the journal paper, to which the PI contributed substantially in the first year of the contract, is attached.

The conference paper titled *Implications of Coronal Abundance Variations*, by Julia L.R. Saba and Keith T. Strong, appeared in July in the Proceedings of the Kofu Symposium, "New Look at the Sun with Emphasis on Advanced Observations of Coronal Dynamics and Flares – What Do We See with Yohkoh and Nobeyama Radioheliograph," eds. S. Enome and T. Hirayama, Nobeyama Radio Observatory Report No. 360, 1994. A reprint is attached.

A paper titled *Anomalous Coronal Neon Abundances in Quiescent Active Regions* is being prepared for submission to Astrophysical Journal Letters by J.T. Schmelz, J.L.R. Saba, D. Ghosh, and K.T. Strong.

V. FOREIGN TRAVEL REPORT

During the reporting period, Dr. Saba traveled to Hamburg, Germany, to attend the COSPAR (Committee on Space Research) meeting in Hamburg, Germany (11-21 July 1994) and participate in two solar sessions: a one-day meeting (Session E2.1) on "Element Abundance Variations in the Sun and the Heliosphere," on 16 July and a four-day symposium (Session E2.2) on "Solar Flare, Coronal, and Heliospheric Dynamics," 18-21 July. The first solar session, which Saba helped organize, brought together some of key researchers and the latest results in the rapidly changing field of solar abundances. The talks and the discussions following were extremely useful for understanding various aspects of the coronal abundance picture and where some of the major uncertainties and discrepancies lie.

At this session, Saba gave an invited review paper on spectroscopic measurements of coronal abundances including results from her FCS research to date. Questions and discussion after the talk suggested some areas which need more work or thought and some possible new approaches. Some of these have already been incorporated in the refereed conference

paper, which has been accepted for publication in Advances in Space Research; a preprint is attached. The other solar session, on dynamics, was pertinent to the next stage of Saba's abundance research – an investigation of whether abundance variations are linked with coronal dynamics. This linkage is plausible and would mean that the observed abundance variations might be useful as a probe of conditions deeper in the solar atmosphere, but it remains to be demonstrated by the kind of correlative study planned.

Saba was invited to visit the Service d'Astrophysique, Centre d'Etudes de Saclay, in Gif-sur-Yvette, near Paris, France during the week before the COSPAR meeting, with Saclay underwriting the expenses for the Paris leg of the trip. Saba was hosted there by Dr. Jean-Paul Meyer, who has done extensive work in the field of solar abundances. Saba and Meyer had many intensive, profitable discussions on topics such as approaches for integrating the solar active region and flare abundance results, and reconciling the variable coronal abundances measured spectroscopically with the more stable coronal composition inferred from solar energetic particle measurements; the problem of normalizing abundances relative to hydrogen; the roles played by elemental abundances in other plasma diagnostic measurements, and by line emissivity calculations in the inferred abundances. Some of the insights gained from these discussions were reflected in the COSPAR talk and subsequent paper.

At Saclay, Saba also discussed with Dr. Monique Arnaud the issues involved in calculating ionization balances, and the problems in trying to use the new iron ionization fractions of Arnaud & Raymond (1985) in the FCS abundance analysis. The ionization fractions are an important factor in deriving temperatures and abundances from measured line intensities, and in deconvolving abundance effects from temperature evolution.

Saba flew to Paris from Washington/Dulles on Thursday, 7 July 1994, arrived in Paris Friday morning, and worked at Saclay and at the home of Jean-Paul Meyer through Thursday, 14 July. Thursday evening, she took an overnight train to Hamburg, arriving early Friday morning. She attended the COSPAR meeting through Thursday, 21 July, returned to Paris by overnight train Thursday evening, and then flew to Washington/Dulles on Friday, 22 July.

REFERENCES

Arnaud, M., & Raymond, J. 1992, Astrophys. J., 398, 394

Arnaud, M., & Rothenflug, R., 1985, Astron. Astrophys. Suppl. Ser. 60, 425.

Mason, H.E. 1992, Proc. of the First SoHO Workshop, Annapolis, Maryland, USA, 25-28 August 1992 (ESA SP-348, November 1992).

McKenzie, D.L., & Feldman, U. 1992, Astrophys. J., 389, 764.

Saba, J.L.R., and Strong, K.T., 1993, Adv. Space Res. 13, no. 9, 391.

Schmelz, J.T. Saba, J.L.R., and Strong, K.T., 1992, Astrophys. J., 398, L115.

Strong, K.T., Lemen, J.R., and Linford, G.A. 1991, Adv. Space Res., 11 (1) 151.

Waljeski, K., Moses, D., Dere, K.P., Saba, J.L.R., Strong, K.T., Webb, D.F., Zarro, D.M., 1994, Astrophys. J., 429, 909.

(COSPAR 1994 Paper E2.1-002, invited review to be published in *Advances in Space Research*)

SPECTROSCOPIC MEASUREMENTS OF ELEMENT ABUNDANCES IN THE SOLAR CORONA: VARIATIONS ON THE FIP THEME

J. L. R. Saba

Lockheed Solar & Astrophysics Laboratory, Palo Alto, CA, U.S.A. 94304, (currently at Solar Data Analysis Center, Code 682, NASA/GSFC, Greenbelt, MD 20771, U.S.A.)

ABSTRACT

Solar wind and solar energetic particle (SEP) data yield systematic differences between elemental abundances in the corona and in the photosphere related to the first ionization potential (FIP) of the elements: low-FIP elements are preferentially enhanced relative to high-FIP elements by about a factor of four. Spectroscopic studies of the inner corona show that such a pattern may apply on average but not in detail for coronal loops: substantial abundance differences occur between different types of coronal structures, and variations have been found from flare to flare, from one active region to another, and over time in the same region; further, in some flares, anomalies such as enhanced Ne:O ratios, distinctly at odds with the FIP pattern, show that a competing element selection mechanism sometimes operates. Details of the observed abundance variability – such as the magnitude of the variations, the relevant temporal and spatial scales, and correlations with other properties of the given coronal structure – may give important clues to the processes which supply and heat the corona, or they may reflect the changing physical conditions or locations where those processes take place. However, many such details remain to be established definitively. At present, abundance variability is primarily a major complication to data analysis and interpretation. However, once it is better understood, it may provide a new diagnostic tool for probing the lower layers of the solar atmosphere.

INTRODUCTION

Several recent comprehensive reviews of elemental abundances in the corona have been written /1,2,3,4/. The discussion here concentrates on several of the outstanding problems and inconsistencies in spectroscopic determinations of coronal abundances. A detailed examination of the theoretical calculations and the atomic data needed to transform observed line intensities into abundances is given by H. Mason elsewhere in this issue.

There has been fairly strong spectroscopic evidence for at least 20 years that coronal composition differs from that in the photosphere (e.g., the careful forbidden line study by Mason /5/). Yet many analyses of coronal abundances found results which appeared ambiguous or even contradictory. The discrepancies were due to a variety of sources: inadequacies in the atomic data, in the spectral or spatial resolution, or in incomplete separation of temperature and abundance effects; in some cases, the uncertainties were simply too large for any definitive statements to be made. One possibility that was not at first considered was abundance variability within the corona, discovered for flares by Sylwester, Lemen, and Mewe /6/, and then for active regions by Strong and colleagues /7,8/; variations in composition from one type of coronal structure to another were discovered by Widing and Feldman /9/ and colleagues (see /4/ and references therein).

It is currently difficult to synthesize the existing spectroscopic results into a single coherent picture when some of the most intriguing results appear contradictory and important questions remain to be answered. Still, some broad statements may be made:

(1) There appears to be basic agreement with the SEP and solar wind picture that elemental composition in the corona differs on average from that in the photosphere, with an overall systematic

bias based on first ionization potential (FIP) of the elements, with low-FIP (<10 eV) elements enhanced relative to high-FIP (>11 eV) elements, compared to their photospheric ratios.

(2) The case for abundance variability *within* the corona is very strong. This variability includes systematic variations in average composition from one type of coronal feature to another /9/, variations between flares (e.g., /6,10,11/), variations between active regions /7,8,12,13/, and variability over time in a given active region /8,13/.

In many cases, the variations are consistent with some generalized version of the FIP-based picture, if one allows for variation in the boundary conditions for the element separation mechanism(s), or perhaps for different heights from which source material is drawn into the corona. In some cases, the abundance variability includes effects not consistent with the general FIP-related bias; notably this includes enhancements of neon (a high-FIP element) during certain flares and long-duration events /14,15,16/, which Shemi /17/ explains as being due to preferential photoionization of neon. There is growing spectroscopic evidence that the FIP enhancement factor, rather than being a simple, constant step function, may be a more complicated function /4,18/, or that it may be variable /7,12,13,19,20/. Recent analyses of active region abundances using soft X-ray spectrometer observations from *P78-1* /12/ and *SMM* /13/ suggest that the "coronal" ratios of low-FIP/high-FIP element pairs such as Fe/Ne, Fe/O, Mg/Ne, and Mg/O can vary approximately from their photospheric values to the "SEP coronal" values or even higher.

ABUNDANCE ANALYSIS METHODS

Several kinds of spectroscopic techniques are used to determine coronal abundances. The most commonly used methods and some of their difficulties are discussed here briefly.

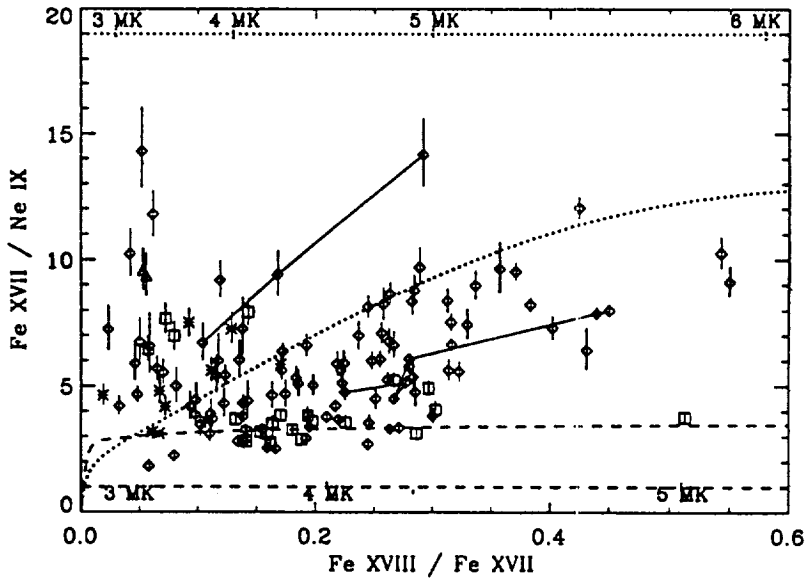

Fig. 1. Abundance-diagnostic ratio Fe XVII/Ne IX plotted vs. temperature parameter, Fe XVIII/Fe XVII. (From Saba and Strong /13/.)

Line Ratios

One technique for determining relative elemental abundances is to use abundance-independent, temperature-diagnostic line ratios, such as the ratios of lines from different ionization stages of iron, to characterize the temperature of the plasma, and then to examine in parallel the flux ratios of lines from different elements, which are temperature-invariant or which vary only slowly with temperature over the relevant temperature regime. An example of this method's use in analysis of FCS data from *SMM* /13/ is shown in Figure 1. Different symbols designate different active

regions observed. Two sequences of measurements taken in the decay phase of long-duration events are connected by solid curves. The line ratios can be converted to abundance ratios by dividing out the temperature dependences of the line emissivity functions. The two different theoretical emissivity curves plotted (dashed and dotted curves), discussed below, imply different conversion algorithms. This method was also used by McKenzie and Feldman /12/, for data from P78-1, and in a series of papers by Widing and Feldman /9,19,21/ and colleagues, for analysis of EUV data from *Skylab*.

The line-ratio technique is dangerous to use blindly, if the shapes of the emissivity functions of the two lines being used for the abundance-diagnostic ratio do not match with good precision in the temperature regime where there is significant emission measure; however, this method is convenient to use and complementary to other methods. In particular, line ratios can provide estimates of relative abundances for use in emissivity curve overlay and for a first guess in differential emission measure (DEM) analyses; consistency checks on the line-ratio method can be made by comparing the results from multiple line ratios, for lines covering a broad range of temperature.

Emissivity Curve Overlay

A more general method than the line-ratio technique is to overlay the emissivity functions for a variety of observed emission lines. This method was applied to soft X-ray data by Strong /22/, and further developed by Veck et al. /23/. If the isothermal approximation is valid, then the curves will intersect in a single emission-measure/temperature solution, to within the uncertainties, provided that the theoretical emissivities are correct and a correct set of abundances is adopted. If the plasma is not isothermal to within the measurement uncertainties, or if an incorrect set of abundances is assumed, the curves will not all overlap in a single location. Figure 2, taken from Veck et al. /23/, shows examples of these two cases. For serious quantitative studies, this method should be accompanied by a rigorous analysis of the uncertainties.

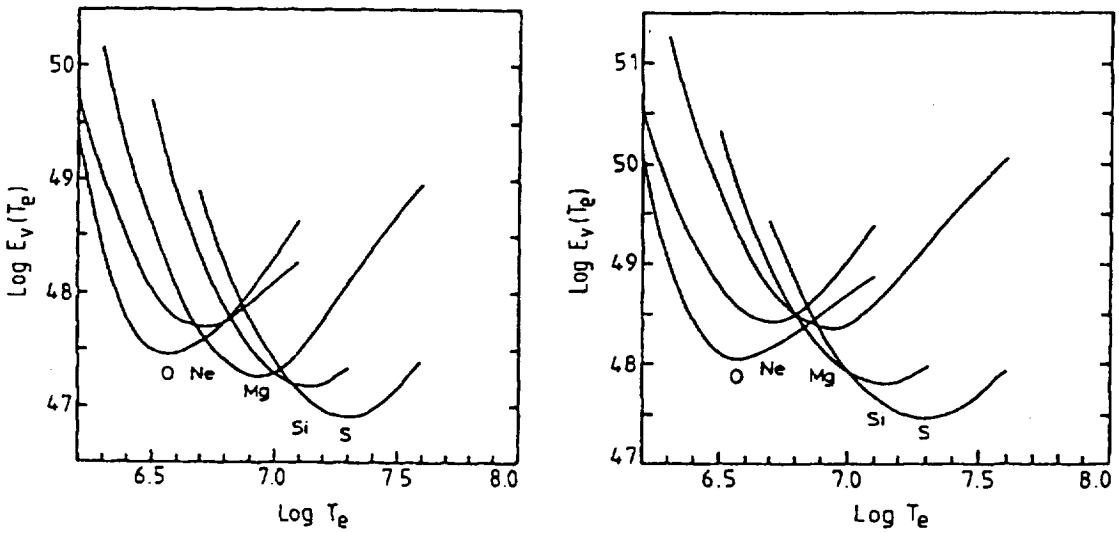

Fig. 2. Overlay of emissivity curves from soft X-ray lines. The left panel shows curves for multithermal plasma during a flare; the right panel shows nearly isothermal plasma during the flare decay. (From Veck et al. /23/.)

The emissivity curve overlay method has been used recently to look for abundance anomalies in *SMM* FCS measurements of active regions, for a set of active regions (see paper by J. Schmelz in this issue), and to determine the composition of a single active region for which soft X-ray broadband data were available in addition to soft X-ray emission line data /24/; the emissivity curves for the broadband data were derived using synthetic spectra at various temperatures for a given set of abundances. In the latter study, Waljeski et al. /24/, compared the results for

isothermal models and for standard empirical Gaussian differential emission measure (DEM) models; the abundance results were found to be indistinguishable.

Differential Emission Measure

If there are enough emission lines, with good temperature coverage and sufficient overlap, it is possible to do a DEM analysis of temperature, which involves an iterative inversion procedure /25/. Since the elemental abundances are not known *a priori*, it is useful to have several lines from different ionization stages of the same element. If the emission lines from other elements can be scaled to match the DEM at the appropriate temperature, the relative elemental abundances can be determined from the normalization adjustment needed to make the different lines mutually consistent. An incorrect set of abundances, or continuing the iteration procedure past the point where the model falls within the one-sigma uncertainties of the data, can introduce artificial complexity into the DEM solution /18/. In general, a full DEM treatment for many spectra may be impractical, but it is possible to examine several cases for general guidance in the data analysis, and to compare the results with synthetic multithermal spectra calculated from first principles for various reasonable physical models.

Line-to-Continuum Studies

This method has been applied almost exclusively to soft X-ray flare studies. If used correctly, for a detector with a low intrinsic background, line-to-continuum intensity ratios can be used to obtain elemental abundances relative to hydrogen. However, there are several additional caveats: The method requires that the emission line and the adjacent (contamination-free) continuum be formed in the same volume; that the plasma be in ionization equilibrium, with a Maxwellian electron velocity distribution; and that the free-bound contribution to the continuum (which itself depends on the coronal composition) be accounted for properly. This last requirement is difficult to meet at temperatures below about 15 MK for wavelengths shorter than about 10 Å, without *a priori* knowledge of the abundances of certain elements (see, e.g., study by Culhane /26/). On the other hand, the method is most accurate for plasmas which are at least approximately isothermal, a condition not typical of flares. Both the free-free and the free-bound continuua depend significantly on the abundance of helium, which is generally unknown or known poorly in the corona (however, see paper by J.L. Culhane et al. in this issue).

The continuum intensity (photon $s^{-1}Å^{-1}$) emitted by an isothermal (Maxwellian) plasma is approximately given by:

$$I_C(T) = \int (G_{ff} + G_{fb} + G_{2\gamma}) T^{-1/2} \lambda^{-1} e^{-E/kT} n_e n_H dV, \qquad (1)$$

where the average Gaunt factors G_{ff}, G_{fb}, $G_{2\gamma}$ represent contributions to the continuum emission from free-free, free-bound, and two-photon processes. The continuum Gaunt factors and the resulting continuum have been calculated by various authors; the calculations by Mewe, Lemen, and van den Oord /27/, which use the cosmic abundances of Allen /28/, are given in a convenient form and have been used in most of the *SMM* and *Yohkoh* analyses. Figure 3 shows plots from Mewe et al. giving the continuum components at plasma temperatures of 10 MK and 20 MK.

At 20 MK, the free-free component dominates; at active region temperatures, the free-bound component is important for wavelengths as large as about 20 Å /26/. At temperatures near 10 MK, for Allen abundances, the free-free and free-bound components are comparable at a few Å /27/. Hence the line-to-continuum method must be used with caution, with a self-consistent treatment of the abundances in the free-bound component, for flare temperatures below about 15 MK and wavelengths below about 10 Å, and perhaps even at higher temperatures and longer wavelengths. If the elements contributing to the local free-bound emission are enhanced (relative to hydrogen) compared to cosmic composition, the free-bound component will be higher than anticipated, leading to artificially low line-to-continuum intensity ratios and hence artificially low abundances relative to hydrogen.

In concentrating on flare decays, in an effort to avoid transient nonequilibrium conditions and minimize nonthermal motions, some *SMM* and *Yohkoh* line-to-continuum studies (e.g., /29/) have included plasma at temperatures where the free-bound component is important, and so may have introduced significant systematic errors. The same problem might also have affected some of the results of Veck and Parkinson /30/.

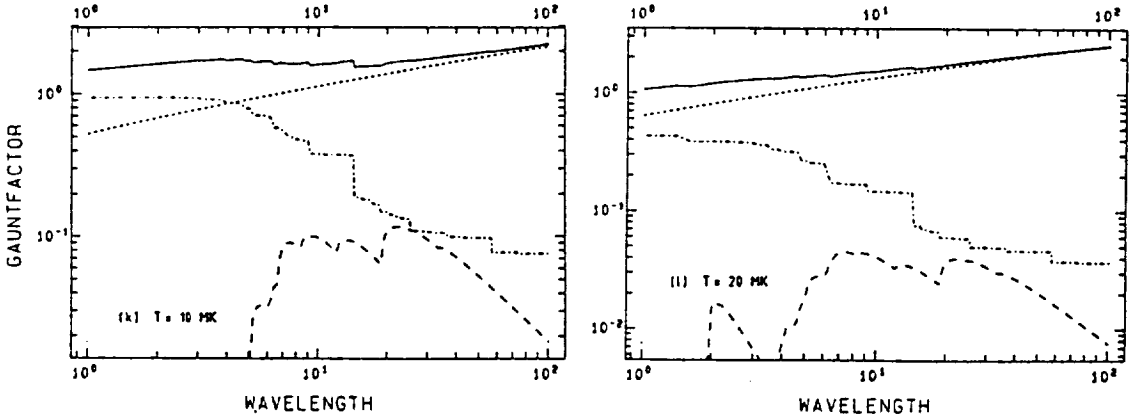

Fig. 3. Relative contributions of free-free (dotted curve), free-bound (dot-dash curve), and two-photon (dashed curve) to the total continuum emission (solid curve) at 10 MK (left) and 20 MK (right), for Allen abundances. (From Mewe et al. /27/.)

There appears to be a systematic difference between the calcium abundance results from *SMM* and from *Yohkoh*, with the *Yohkoh* values falling preferentially at the low end of the *SMM* values, and showing much lower overall variability. Potential sources of this difference are being explored by the *Yohkoh* BCS instrument team members, many of whom were also previously involved in *SMM* BCS analyses. One possibility which is being explored is that the "flare continuum" in the *Yohkoh* BCS instrument is contaminated by cooler solar flux from regions not involved in the flare /31/; one of the main differences between the *SMM* and *Yohkoh* BCS instruments is the differing fields of view – the *SMM* BCS has a 6 arc minute (FWHM) field of view, while the *Yohkoh* BCS views the whole Sun.

Optical Forbidden-Line Equivalent Width

Pottasch /32/ describes the procedure for determining absolute abundances from the equivalent width of optical coronal forbidden lines. Conceptually, this method is similar to the line-to-continuum method described above, but the implementation and caveats are different. The visible continuum in the lower corona is produced almost entirely by electron scattering of photospheric radiation /32/. Hence the primary concerns are determining the electron density in the same region as that where the equivalent width is measured, and removing the effects of line-of-sight averaging of the emission line in the optically thin corona. One uses statistical equilibrium equations to calculate the number of ions in all levels from the population of the upper level, which requires accurate transition probabilities and electron collisional excitation rates. Then one sums all of the different ionization stages of the given element, which requires knowledge of the temperature distribution and accurate ionization balance calculations. Using this method, Pottasch /32/ found an abundance ratio of Fe/H = 8×10^{-5}, about 2.5 times the current estimate of the photospheric value. With greatly improved atomic data from detailed calculations including cascades, Mason /5/ found similar coronal enhancements of Ca/H and Fe/H in a coronal condensation.

Generalized DEM

Fludra et al. /11/ proposed a method which combines the well known technique of using line ratios of the Ca XIX and Fe XXV resonance lines w and their dielectronic satellites k and j, respectively /33/, with standard multi-temperature analysis /34/; the generalized method uses line fluxes and line flux ratios simultaneously to derive the DEM to obtain relative abundances or the absolute abundance if continuum flux for one of the lines is also included in the analysis. This method is especially useful for obtaining the Fe/Ca and the Fe/H abundance in flares observed by the *SMM* BCS. (A background resulting from fluorescence of germanium crystals contributes a significant, time-variable proportion of the total background in the *SMM* BCS iron channel, while the *SMM* Ca XIX background is generally regarded as free of contamination.)

ASSUMPTIONS

A variety of assumptions go into abundance analyses of coronal spectroscopic data. Generally the plasma is assumed to be optically thin, at least to absorption, and typically to electron scattering as well. The plasma is assumed to be in ionization equilibrium; in flare studies this assumption may not be valid in the impulsive phase, which is therefore usually excluded from the analysis. The electron velocity distribution is assumed to be Maxwellian. Whenever a line ratio or line-to-continuum ratio is taken, an implicit assumption is made that the emissions being compared come from the same volume(s). On the other hand, Jakimiec et al. /35/ point out that the volume of plasma which produces flare continuum emission may be larger than that which produces flare line emission if the electron mean free path is large enough to allow electrons to escape from the high-temperature volume before interacting with the highly ionized calcium and iron atoms. In effect, this means that the electron distribution which produces the line emission might have a *depleted* high-energy tail, which would result in lower observed values of coronal abundances.

Theoretical emissivity calculations

To convert relative line intensities to relative abundances or line-to-continuum or equivalent-width measurements to absolute abundances requires modeling of the emission line and continuum emissivities as a function of temperature and knowledge of the temperature distribution of the emitting plasma. The theoretical calculations of emissivities are discussed in detail in a review elsewhere in this issue. Here some general aspects of the calculations are discussed.

In the "coronal approximation" of a low-density plasma in thermodynamic equilibrium, the emissivity function of an emission line is essentially a product of the elemental abundance times two temperature-dependent factors: the fraction of the emitting element in the relevant ionization stage (the ionization fraction) and the probability that the ion will make the given transition to produce the line (which depends on the level population and the excitation rate). For the H-like and He-like lines, the level populations and excitation rates are believed to be well understood. Multielectron ions, such as the neon-like Fe XVII and fluorine-like Fe XVIII resonance lines are harder to model, but the excitation rates are believed to be known to about 30% /36/. The ionization fractions, especially for multi-electron ions, are more difficult to calculate and correspondingly more uncertain.

A variety of calculations of equilibrium ionization balance have been made; differences in the calculations change the slope and the absolute scaling of the net line emissivity functions, which in turn affect the theoretical line or line-to-continuum ratios and hence the derived values of abundances. If the calculated ionization balance is in error, the derived abundances may show some apparent temperature dependence. A lack of ionization equilibrium would also change the ionization fractions. However, currently accepted flare models and densities point to ionization equilibrium during most of a flare, except perhaps the early rise phase /37/. Disagreement of various existing ionization balance calculations for calcium or iron with observed X-ray spectra has been reported previously by many authors, and empirical corrections have been proposed by some of them (e.g., /10,11,38,39/). None of the empirical corrections explain fully all observed line-to-line or line-to-continuum ratios, and they should be regarded with caution.

Recent calculations of iron ionization fractions by Arnaud and Raymond /40/ [hereafter, ARA] in some cases give significantly different results from previous calculations by Arnaud and Rothenflug /41/ [hereafter, ARO], as shown by the two theoretical curves in Figure 1, which predict very different temperature behaviour for Fe XVII/Ne IX. The ARO calculations predict that this line ratio should be very flat over the temperature regime relevant for active regions, while the ARA calculations predict an increase with temperature. In comparisons with data from the *SMM* FCS, the new ARA calculations appear less consistent than the older ARO calculations for Fe XVII and Fe XVIII in the regime of a few MK /13/. However, it remains to be seen whether the apparent difficulties with the ARA calculations are in fact due instead to effects of resonant scattering or inadequate calculations for the Fe XVII or Fe XVIII excitation rates. It should be noted that, while the two calculations give different boundaries for the range of Fe/Ne variability, the overall magnitude of the variability is comparable; also, while the ARA calculations imply that the variations on timescales less than an hour are due to temperature evolution rather than a change in abundance, day-to-day changes in the active region abundances remain.

Optically thin emission

Although coronal emission lines are generally thought to be optically thin, results from a recent reconsideration of radiative transfer of Fe XVII in the corona suggest that resonance scattering might be responsible for the observed depletion of flux (relative to other bright emission lines) in the Fe XVII resonance line at 15.01 Å in active regions /42/.

In resonance scattering, a resonance line photon is absorbed by an ion in the ground state and then re-emitted, generally in a different direction. This absorption and re-emission is indistinguishable from scattering and depends on the geometry of the region being observed. In general, photons would be preferentially scattered out of the line of sight for relatively dense, bright areas, as compared to fainter surrounding areas. The absorption coefficient for resonance scattering, as given by Acton /43/ for $J = 1 \rightarrow 0$ transitions, is

$$\kappa_0 = 9.31 \times 10^{-18} f_{lu} A_i A n_e \lambda_A M^{1/2} T_e^{-1/2}, \tag{2}$$

where f_{lu} is the absorption oscillator strength, A_i is the temperature-dependent relative abundance of the ion, A is the elemental abundance relative to hydrogen, n_e is the density, λ_A is the wavelength in Å, M is the mass in atomic mass units, and T_e is the ion temperature in units of 10^6 K. The corresponding opacity at line center is

$$\tau_0 = \int \kappa_0 dL, \tag{3}$$

where dL is the line-of-sight element. If resonance scattering is in fact responsible for the apparent flux reduction of the Fe XVII line at 15.01 A, then it must be taken into account in deriving relative abundances from the measured line flux ratios, or other unaffected lines must be used to avoid systematic effects in the derived values of relative abundances. It is important to determine if resonance scattering does play a major role in the FCS and in other data sets for reasonable coronal parameters.

NORMALIZATION OF ABUNDANCES

A key issue is whether the low-FIP elements are enhanced or the high-FIP elements are depleted (or both) in the corona relative to their photospheric values. The absolute normalization of abundances is important both for determining the amount of source material producing a given line intensity and also for modeling the element separation mechanism(s) responsible for the differences between photospheric and coronal composition. Since the bulk of the plasma is hydrogen, the question hinges on the behavior of elements relative to hydrogen. The solar wind and SEP observations seem to imply that the low-FIP elements are enhanced in the corona by a factor of 3 to 4 while the high-FIP elements have their photospheric values. A variety of acceleration and transport processes may treat protons (i.e., ionized hydrogen) differently than heavier ions, so that heavy ion-to-proton ratios may not directly reflect the coronal heavy element-to-hydrogen

composition. Hence, it is desirable to have independent information from the spectroscopic abundance measurements. Unfortunately, at present, the spectroscopic results are not consistent.

In the upper chromosphere, transition region, and corona, the temperature is above 3×10^4 K, hence hydrogen is essentially fully ionized, and therefore has no emission lines. Thus, most abundance studies of emission lines from these regions give their results in terms of relative abundances. Recent EUV spectroscopic abundance results have been interpreted to mean that the low-FIP elements are enhanced exactly as in the SEP/solar wind picture /4/. However, while the arguments are plausible, they are somewhat indirect and involve comparison of lines from different temperature regimes. Line-to-continuum and equivalent-width analyses give direct measures of abundances relative to hydrogen, subject to the caveats listed above. However, the line-to-continuum measurements show a large range of results, from a factor of 4 enhancement of low-FIP elements /44/, to factor of two or less enhancement of low-FIPs, accompanied by a factor of two depletion of high-FIPs /18,30/. Some of these measurements may be compromised by inadequate treatment of the free-bound continuum, or by contamination of the continuum by solar or nonsolar flux. Equivalent-width studies have shown factor of 2 to 3 enhancement of low-FIP elements /5,32/. Now that there are better atomic data available, it would be useful to examine more of the eclipse forbidden line data sets.

Two novel approaches have been suggested recently for determining absolute coronal abundances. In the first of these (see paper by K. Phillips et al. elsewhere in this issue), Phillips et al. /45,46/ compared the intensities of Fe Kα and Kβ lines (which they argue are formed principally by fluorescence in the photosphere) to the Fe XXV resonance line (produced by hot flare plasma in the low corona). They deduced that the Fe/H coronal abundance ratio is not more than a factor of two higher than photospheric for a large sample of different kinds of flares observed by *SMM* BCS, *P78-1* SOLEX or *Yohkoh* BCS. It is not clear if this result could be affected by an underestimation of the free-bound component of the continuum emission, as discussed above for line-to-continuum studies. The possibility should also be considered that the Fe Kα and Kβ lines are formed at heights considerably above the photosphere, where the element differentiation has already occurred. Still, if these potential complications can be ruled out, this result implies that the low-FIP elements are not greatly enhanced in the corona.

The second new method proposes to exploit resonance scattering of a bright Fe XVII line at 15.01 Å to get absolute abundances in active regions. With this method, using *SMM* FCS emission line intensities and AS&E broadband X-ray image data for information on geometry, Waljeski et al. /24/ found Fe:H = $3.2 \times 10^{-4}(\pm 60\%)$, about 10 times the photospheric value. In this method, the effective optical depth at line center, τ, to scattering is determined from the observed flux depletions of a pair of the Fe XVII lines and then also calculated from equations (2) and (3). For a line unaffected by resonance scattering, the line intensity is directly proportional to the factor Fe/H times the volume emission measure, $\mathrm{EM} = \int n_e^2 dV$, where dV is the elemental volume (times factors involving atomic data and constants). For uniform density, $\int n_e dl \simeq n_e L$ and $\int n_e^2 dV \simeq n_e^2 La$, where a is the cross-sectional area and L is the path length, which can be estimated from imaging data. Making the substitution $\int n_e dL \simeq [\int n_e^2 dV]/[n_e a]$ in the equation for τ allows one to solve for Fe/H.

Unfortunately, even if it is confirmed that resonance scattering is the sole source of the discrepancy between measured and predicted fluxes for the Fe XVII line at 15.01 Å, there are currently two problems with using this approach: (1) the resonance scattering process in the active region geometry needs to be modeled more exactly to derive the calculated opacity to an accuracy better than about a factor of two; and (2) the required substitution of the volume emission measure term for the integrated column density neglects a geometric term which is roughly proportional to $L \times f_L/f_A$, where f_L and f_A are the volume and area filling factors, respectively. Thus the net systematic uncertainty could easily be comparable in magnitude to the low-FIP/high-FIP enhancement factor in the corona. These difficulties may be be overcome with future observations which combine direct information on the appropriate geometric model (from high-resolution imaging) and independent information on the electron density, from a density-diagnostic line ratio

(which must be appropriate for the temperature regime of formation of the resonantly scattered line).

CONCLUSIONS

Although a large amount of recent work has led to many interesting new results, the state of spectroscopic measurements of coronal abundances is not as mature as that of the solar energetic particle (SEP) and solar wind measurements. There remain ambiguities and contradictions in the spectroscopic coronal abundance results. The basic uncertainties include: discrepancies between different instruments and different analysis techiques on absolute abundances, and discrepancies between different instruments on the degree of abundance variability between and within flares. Our knowledge is currently sparse in several important areas: the relevant temporal scales and spatial scales for abundance variability in nonflaring regions, and the degree and nature of variability in low-FIP/low-FIP and high-FIP/high-FIP pairs of elements. We still lack basic observational information on the distribution of abundances with height. We do not yet know how to relate the spectroscopic and SEP results. All of this information is needed to provide realistic constraints on models of the element selection mechanism(s) responsible for the differences in composition between the photosphere and the corona.

Although we are still disentangling the detailed effects of variable abundances from the effects of uncertainties in the emissivity calculations and physical modeling, it is clear that significant coronal abundance variations occur. There are many cases for which the apparent variations are much larger than the uncertainties, which cannot be explained in terms of problems with emissivity calculations or the presence of multithermal plasma. Continuing work on the theoretical predictions for line emissivities (particularly the ionization fractions), on accurate modeling of continuum emission (particularly the abundance dependence of the free-bound component), and on reasonable physical modeling of the geometry and multithermal distribution of plasma is needed to derive the details of the abundance variations required to challenge physical models.

ACKNOWLEDGEMENTS

Preparation of this review and travel to the COSPAR meeting was supported by NASA contract NASW-4814. The author has benefited greatly from working on abundances with Keith Strong, from many discussions on abundances with Andrzej Fludra, Joan Schmelz, Don Reames, and Jean-Paul Meyer, and from the insights shared on emissivity calculations and modeling by Helen Mason, Anand Bhatia, and Alan Gabriel. Most of the *SMM* results discussed here could not have been obtained without the repair of the *SMM* spacecraft by the crew of the *Challenger* on mission 41-C. This paper is dedicated to the memory of Francis R. Scobee, the pilot for that mission, and the commander of *Challenger's* last flight.

REFERENCES

1. Meyer, J.P. *Adv. Space Res.*, **11**, (1)269 (1991).
2. Meyer, J.P., *Adv. Space Res.*, **13**, (9)377 (1993).
3. Meyer, J.P., in *Origin and Evolution of the Elements*, eds. N. Prantzos, E. Vangioni-Flam, and M. Casse, Cambridge University Press (1993).
4. U. Feldman, *Physica Scripta*, **46**, 202 (1992).
5. H.E. Mason, *Mon. Not. R. astr. Soc.*, **171**, 119 (1975).
6. J. Sylwester, J.R. Lemen, R. Mewe, *Nature*, **310**, 665 (1984).
7. K.T. Strong, E.S. Claflin, J.R. Lemen, and G.A. Linford, *Adv. Space Res.*, **8**, (11)167 (1988).
8. K.T. Strong, J.R. Lemen, and G.A. Linford, *Adv. Space Res.*, **11**, (1)151 (1991).
9. K.G. Widing and U. Feldman, 1989, *Astrophys. J*, **344**, 1046 (1989).
10. J.R. Lemen, J. Sylwester, and R.D. Bentley, *Adv. Space Res.*, **6**, (6)245 (1986).
11. A. Fludra, A., Bentley, R.D., Culhane, J.L., Lemen, J.R., and Sylwester, J., *Adv. Space Res.*, **11**, (1)1155 (1991).

12. D.L. McKenzie and U. Feldman, *Astrophys. J*, **389**, 764 (1992).
13. J.L.R. Saba and K.T. Strong, *Adv. Space Res.*, **13**, 9(394) (1993).
14. R.J. Murphy, R. Ramaty, B. Kozlovsky, and D.V. Reames, *Astrophys. J.*, **371**, 793 (1991).
15. J.T. Schmelz and A. Fludra, *Adv. Space Res.*, **13**, (9)325, 1993.
16. J.T. Schmelz, *Astrophys. J.*, **408**, 373. (1993).
17. A. Shemi, *Mon. Not. R. astr. Soc*, **251**, 221 (1991).
18. A. Fludra and J.T. Schmelz, *Astrophys. J.*, submitted, 1994.
19. K.G. Widing, and U. Feldman, *Astrophys. J.*, **392**, 715 (1992).
20. D. Falconer, Ph.D. thesis, U. Maryland, 1994.
21. U. Feldman and K.G. Widing, *Astrophys. J.*, **363**, 292 (1990).
22. K.T. Strong, Ph.D. thesis, University College London (1978).
23. N.J. Veck, K.T. Strong, C. Jordan, G.M. Simnett, P.J. Cargill, and E.R. Priest, *Mon. Not. R. astr. Soc.*, **210**, 443 (1984).
24. K. Waljeski, D. Moses, K.P. Dere, J.L.R. Saba, K.T. Strong, D.F. Webb, and D.M. Zarro, *Astrophys. J.*, **429**, 909 (1994).
25. G.L. Withbroe, *Sol. Phys.*, **45**, 301 (1975).
26. J.L. Culhane *Mon. Not. R. astr. Soc.*, **144**, 375 (1969).
27. R. Mewe, J.R. Lemen, and G.H.J. van den Oord, *Astron. Astrophys. Suppl. Ser.*, **65**, 511 (1986).
28. C.W. Allen, *Astrophysical Quantities* (London:Athlone) (1976).
29. A. Fludra, R.D. Bentley, J.L. Culhane, G.A. Doschek, E. Hiei, K.J.H. Phillips, A. Sterling, and T. Watanabe, *Adv. Space Res.*, **13**, (9)395 (1993).
30. N.J. Veck and J.H. Parkinson, *Mon. Not. R. astr. Soc.*, **197**, 41 (1981).
31. J.L. Culhane, public comment at the 1994 COSPAR meeting, Hamburg, Germany.
32. S.R. Pottasch, *Mon. Not. R. astr. Soc*, **125**, 543 (1963).
33. A.H. Gabriel, *Mon. Not. R. astr. Soc.*, **160**, 99 (1972).
34. A. Fludra and J. Sylwester, *Solar Phys.*, **105**, 323 (1986).
35. J. Jakimiec, P. Preś, A. Fludra, R.D. Bentley, J.R. Lemen, R. Mewe, J. Schrijver and J. Sylwester, *Adv. Space Res.*, **8**, (11)231 (1988).
36. F. Bely-Dubau, private communication (1992).
37. R. Mewe, J.R. Lemen, G. Peres, J. Schrijver, and S. Serio *Astron. Astrophys.*, **152**, 229 (1985).
38. E. Antonucci, D. Marocchi, A.H. Gabriel, and G.A. Doschek, *Astron. Astrophs.*, **188**, 159 (1987).
39. E. Antonucci, M.A. Dodero, A.H. Gabriel, K. Tanaka, and J. Dubau, *Astron. Astrophys.*, **180**, 263 (1987).
40. M. Arnaud and J. Raymond, *Astrophys. J.* **298**, 394 (1992).
41. M. Arnaud and R. Rothenflug, *Astrophys. J. Suppl.* **60**, 425 (1985).
42. J.T. Schmelz, J.L.R. Saba, and K.T. Strong, *Astrophys. J. (Lett.)*, **398**, L115 (1992).
43. L.W. Acton, *Astrophys. J*, **225**, 1069 (1978).
44. J.R. Lemen and J. Sylwester, private communication, 1993.
45. K.J.H. Phillips, C.D. Pike, J. Lang, Te. Watanabe, and D.M. Zarro, *Proc. of the Kofu Symposium*, Nobeyama Radio Observatory Report No. 360, 301 (1994).
46. K.J.H. Phillips, C.D. Pike, J. Lang, Te. Watanabe, and M. Takahashi, *Astrophys. J.*, in press, 1994.

THE ASTROPHYSICAL JOURNAL, 429:909–923, 1994 July 10

THE COMPOSITION OF A CORONAL ACTIVE REGION

K. WALJESKI,[1,2] D. MOSES,[3] AND K. P. DERE[1]
Naval Research Laboratory, Washington, DC 20375-5352
J. L. R. SABA[4] AND K. T. STRONG
Lockheed Solar and Astrophysics Laboratory, 3251 Hanover Street, Palo Alto, CA 94304
D. F. WEBB
Institute for Space Research, Boston College, 885 Centre Street, Newton, MA 02159
AND
D. M. ZARRO[4]
Applied Research Corporation
Received 1993 July 6; accepted 1994 January 12

ABSTRACT

The relative abundances of iron, oxygen, magnesium, and neon in a coronal active region are determined from measurements of soft X-ray line and broadband intensities. The emission measure, temperature, and column density are derived from these measured intensities and are used to place a constraint on the abundances of the heavier elements relative to hydrogen in the corona.

The intensity measurements were made on 1987 December 11, when an active region was observed jointly by the American Science and Engineering (AS&E) High Resolution Soft X-Ray Imaging Sounding-Rocket Payload and the X-Ray Polychromator Flat Crystal Spectrometer (FCS) onboard the *Solar Maximum Mission* spacecraft. The coordinated observations include images through two broadband filters (8–29 Å and 8–39, 44–60 Å) and profiles of six emission lines: Fe XVII (15.01 Å), Fe XVII (15.26 Å), O VIII (18.97 Å), Mg XI (9.17 Å), Ne IX (13.44 Å), and Fe XVIII (14.21 Å).

The effects of resonance scattering are considered in the interpretation of the FCS line intensities. We calculated the expected intensity ratio of the two Fe XVII lines as a function of optical depth and compared this ratio with the observed intensity ratio to obtain the optical depths of each of the lines and the column density.

The line intensities and the broadband filtered images are consistent with the emission from a thermal plasma where Fe, O, Mg, and Ne have the "adopted coronal" abundances of Meyer (1985b) relative to one another, but are not consistent with the emission from a plasma having photospheric abundances: The ratios of the abundances of the low first ionization potential (FIP) elements (Fe and Mg) to the abundances of the high-FIP elements (Ne and O) are higher than the ratios seen in the photosphere by a factor of about 3.5. This conclusion is independent of the assumption of either an isothermal or a multithermal plasma.

The column densities derived from the Fe XVII line ratio and the geometry of the active region provide a diagnostic of the abundance of hydrogen relative to the heavier elements. We find that the abundance of iron with respect to hydrogen in the corona is higher than the value given Meyer (1985b) by a factor of 8.2 (-5.4, $+5.1$). This means that, for the observed active region, the absolute abundances of the low-FIP elements (Fe and Mg) are enhanced in the corona relative to the photosphere, while the abundances of the high-FIP elements (Ne and O) are either slightly enhanced in the corona or nearly the same in the photosphere and the corona.

Subject headings: Sun: abundances — Sun: activity — Sun: X-rays, gamma rays

1. INTRODUCTION

Knowledge of the composition of the corona is an important key to our understanding of the physical processes of the solar atmosphere. The coronal elemental abundances reflect in some manner the way in which solar plasma is transported, accelerated, and heated. The composition of the corona must also be known in order to interpret observations of coronal emission: The relative abundances of the heavy elements must be known to determine temperature from the intensity ratios of coronal lines of different elements, while the absolute abundances (the abundances of the heavier elements with respect to hydrogen) must be known to determine emission measure and radiation loss.

In this study, broadband images and emission intensities of a coronal active region are used to constrain the relative and absolute abundances of Fe, O, Mg, and Ne. The relative abundances are measured by comparing the observed line and broadband intensities with the intensities that would be expected from model plasmas of a specific composition. The optical depths of the Fe XVII lines and the geometry of the region provide the additional information necessary to determine absolute abundances.

1.1. *Relative Abundances of* Fe, Mg, O, *and* Ne

There is considerable evidence, from in situ solar wind (reviewed by Geiss 1982) and solar energetic particle measure-

[1] Code 7663.
[2] NRC Postdoctoral Research Associate.
[3] Code 7660.
[4] Postal address: Code 682, NASA Goddard Space Flight Center, Greenbelt, MD 20771.

ments (e.g., Brenneman & Stone 1985; Meyer 1985a), as well as from coronal spectroscopic measurements (e.g., Veck & Parkinson 1981; Widing & Feldman 1989), that the compositions of the solar corona and the solar wind differ in a systematic way from the composition of the photosphere. Meyer (1985b) synthesized the abundance measurements published by a large number of investigators. On the basis of this observational evidence, Meyer (1985b) proposed that the composition of the corona and solar wind is fractionated according to first ionization potential (FIP), so that the ratio of the abundances of the low-FIP elements to the abundances of the high-FIP elements is higher in the corona and the solar wind than in the photosphere. Meyer (1985b) presented a set of "adopted coronal" abundances, which differed from the photospheric abundances in that the ratios of the abundances of the low-FIP elements to the abundances of the high-FIP elements were higher in the corona than in the photosphere by a factor of about 3.5.

In this paper, we compare the intensity observations to the emission expected from plasmas with two sets of relative abundances: photospheric abundances (from Grevesse & Anders 1991 with the more recently determined photospheric iron abundance from Grevesse, Noels, & Sauval 1992) and FIP-fractionated "adopted coronal" abundances (Meyer 1985b). Although the observed active-region plasma is contained by closed magnetic loops that are connected to the photosphere, we find that the observed intensities are not consistent with a plasma having photospheric abundances. The observations are consistent with thermal plasmas having the FIP-fractionated adopted coronal relative abundances of Meyer (1985b).

Previous studies of Flat Crystal Spectrometer (FCS) data (e.g., Nitta et al. 1991; Saba & Strong 1991) have shown that some active-region spectra were more consistent with Meyer's adopted coronal relative abundances than with photospheric abundances; however, the present comparison of FCS spectra and broadband filter data gives a more rigorous quantitative basis for this conclusion.

1.2. *Absolute Abundances*

Once the relative abundances of the high-FIP and low-FIP heavy elements have been established, a measurement of the hydrogen abundance is necessary to determine whether the high-FIP elements are underabundant in the corona relative to the photosphere or whether the low-FIP elements are overabundant. On the basis of spectroscopic observations of line and continuum emission from the corona (Veck & Parkinson 1981), Meyer (1985b) concluded that the abundances of the high-FIP elements were depleted in the corona relative to the photosphere. However, recent evidence, reviewed by Meyer 1993a, b) and Feldman (1992), suggests that the abundance of hydrogen relative to the heavier elements is lower than predicted by Meyer (1985b), so that the low-FIP elements are overabundant in the corona.

There is no separate measurement of the continuum in our set of line and broadband observations from which to directly measure the abundance of hydrogen. The broadband filtergrams have the highest contribution of continuum to the signal. However, for all of the filtergram images, the continuum is expected to contribute less than 20% of the total filtered spectrum for emission from plasma at active-region temperatures with the adopted coronal abundances (Meyer 1985b).

The effects of optical depth on the Fe XVII lines are used here as a diagnostic of absolute abundance. Most previous studies have assumed that the corona is optically thin to soft X-rays. As Acton (1978), Rugge & McKenzie (1985), and Schmelz, Saba, & Strong (1992) suggested, we find that the optical depth of the lines must be considered in the analysis of these broadband and line intensities. The intensity ratio of the two Fe XVII lines (15.01 Å/15.26 Å), which differ significantly in oscillator stength, is used as an optical depth diagnostic. Significant optical depths are found for these two Fe XVII lines, the O VIII line (18.97 Å), and the Ne IX line (13.44 Å). The optical depth of the Fe XVII line at 15.01 Å has been proposed as a density diagnostic by Schmelz et al. (1992). Here, we use the column densities, $\int n_e\, dl$, together with the emission measures, $\int n_e^2\, dl$, of coronal soft X-ray lines to provide information on the abundance of hydrogen.

The abundances of the heavier elements relative to hydrogen are found to be a factor of 8.2 ($+5.4$, -5.0) higher than the abundances tabulated by Meyer (1985b), implying that hydrogen behaves as a high-FIP element in the corona. Therefore, the abundances of the low-FIP elements are enhanced in the corona relative to the photosphere, while the abundances of the high-FIP elements, including hydrogen, are nearly the same.

2. OBSERVATIONS

On 1987 December 11, a solar active region, with NOAA designation AR 4901, was observed simultaneously by the American Science and Engineering (AS&E) High Resolution Imaging Sounding-Rocket Payload and the X-Ray Polychromator Flat Crystal Spectrometer (FCS) onboard the *Solar Maximum Mission* (*SMM*) spacecraft. The active region was located near the southwest limb of the Sun, at approximately S22 W72.

2.1. *Spectrometer Observations*

The FCS, described by Acton et al. (1980), consisted of seven rotatable Bragg crystal spectrometers that were able to simultaneously observe the same field of view. The 1987 December 11 observations were all obtained with the first and third crystal channels.

The response of the FCS collimator to an infinite uniform-brightness source was approximately pyramidal, with a full width of 30". Each flux measurement made by the FCS is the convolution of this field response function with the intensity of the source.

Two types of observations were made during the *SMM* satellite orbit (17:55 UT to 18:30 UT) of the AS&E sounding-rocket flight: maps of line peak intensity and spectral scans of line profiles. The maps were made by holding the angle of incidence of the FCS crystals fixed, to select a wavelength at the peak of a chosen soft X-ray emission line, and then rastering the instrument pointing to scan an area of interest at a fixed wavelength. Line profile measurements were made by holding the pointing fixed and rotating the crystals to scan a region of the soft X-ray spectrum near the wavelength of a chosen line.

The FCS observed the brightest area of the active region of interest, at wavelengths around five different emission lines: Fe XVII (15.01 Å), O VIII (18.97 Å), Mg XI (9.17 Å), Ne IX (13.44 Å), and Fe XVIII (14.21 Å). These lines were chosen because they are among the brightest soft X-ray lines within the FCS spectral range (about 1.4–22.4 Å) that are produced by quiet active-region plasmas. A peak intensity map and then a line

profile observation were made for each line, in the order that the lines are listed. In all, six line profiles were measured, because a second Fe XVII line at 15.26 Å was included in the line scan near the Fe XVII line at 15.01 Å. The observations ended with a second Fe XVII (15.01 Å) map, which was only partially completed at the end of the *SMM* orbital day.

2.1.1. *FCS Intensity Maps*

The FCS maps are shown in Figure 1. They range in size from 2′ to 4′ on a side, with raster step intervals of 10″. The maps are of raw counts per second, displayed on a square-root scale.

Comparison of the first and last maps (both Fe XVII maps) shows changes in the active region over the time of FCS observation. The region brightened in this approximately 30 minute time interval. There were 94 raw counts in the brightest pixel of the first Fe XVII map, while the number of counts at the corresponding position in the last Fe XVII map was about 50% higher. The structure of the active region did not change significantly between the first and last maps.

2.1.2. *FCS Spectral Line Scans*

The FCS line profile observations were made at the position of the brightest pixel in the first Fe XVII intensity map. The transitions producing each line are listed in Table 1. The O VIII line results from two different transitions, identified as $1s^2S_{1/2}-2p^2P_{1/2}$ and $1s^2S_{1/2}-2p^2P_{3/2}$. The energies of these two transitions are so close together that they cannot be distinguished from one another in these observations, and so they are treated as one line. The Fe XVIII line is also a result of two transitions, identified by Cornille et al. (1992) as $2p^5\,^2P_{3/2}-2p^4\,3d\,^2D_{5/2}$ and $2p^5\,^2P_{3/2}-2p^4\,3d\,^2P_{3/2}$. The wavelengths of the two Fe XVIII lines are 14.203 Å and 14.215 Å (Fawcett 1984). To simplify the analysis, these two overlapping lines are treated as one line at the average wavelength of 14.21 .

A line flux is determined by fitting the observed line spectrum with a background level and a Voigtian line profile. The assumed line shape is the convolution of the Lorentzian FCS instrument response with the Gaussian shape characteristic of a Doppler-broadened line. The Fe XVIII and O VIII lines are

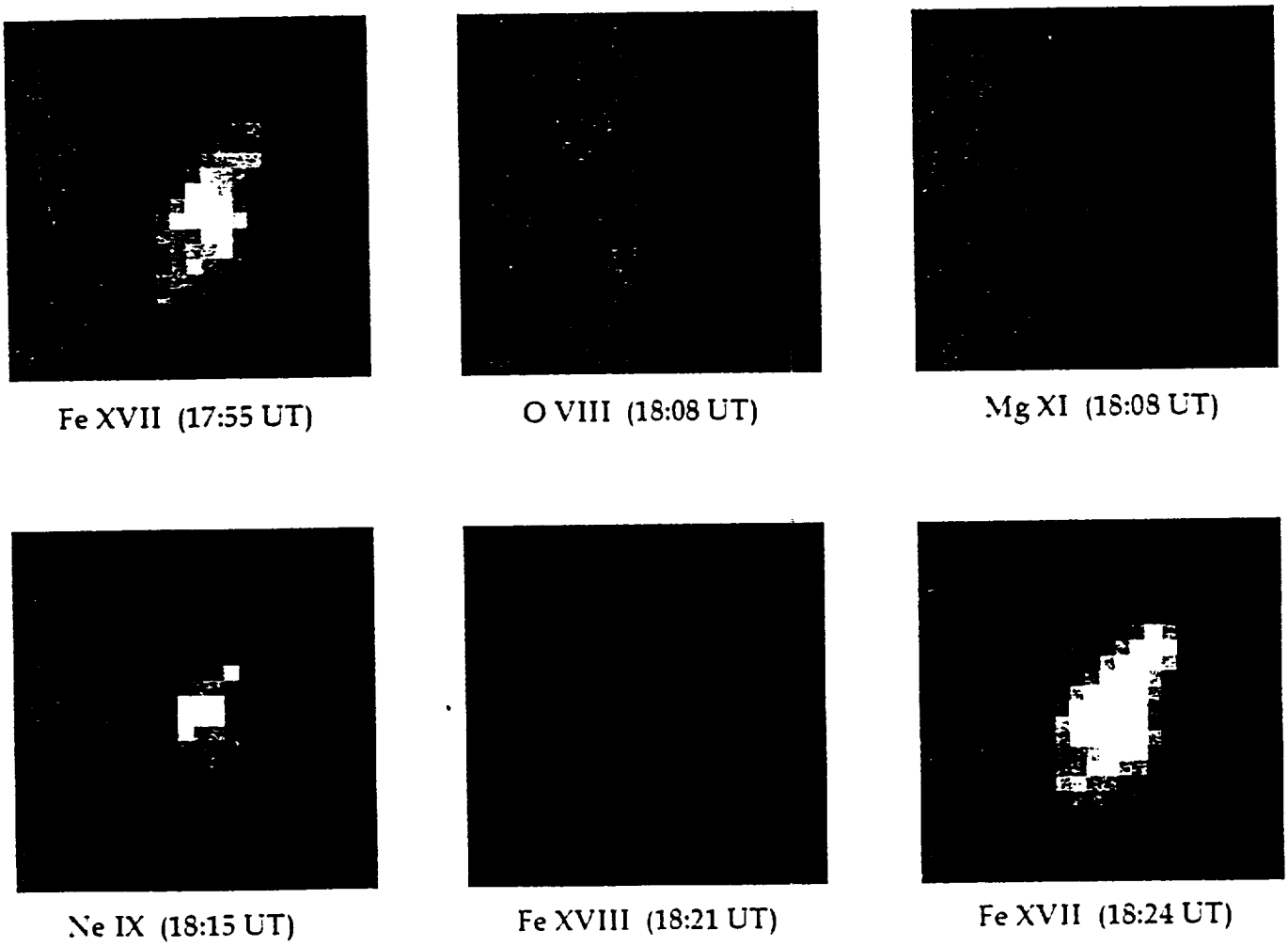

FIG. 1.—FCS line peak intensity maps of AR 4901 between 18:06 and 18:24 UT on 1987 December 11. The starting time of the raster is listed below each map. The first Fe XVII (15.01 Å) raster covers 4′ × 4′. The O VIII (18.97 Å), Mg XI (9.17 Å), Ne IX (13.44 Å), and second Fe XVII (15.01 Å rasters cover 3′ × 3′, and the Fe XVIII (14.21 Å) raster, 2′ × 2′. All the maps are aligned relative to one another and have the same scale, with a step size of 10″. The boxes around each map have dimensions of 4′ × 4′. The last Fe XVII map is incomplete, since the *SMM* satellite day ended before the raster was completed. The images are scaled as the square root of the number of raw counts, with a maximum of 100 counts. The number of raw counts in the central pixel of each map is (1) first Fe XVII map, 94 counts; (2) O VIII maps, 34 counts; (3) Mg XI map, 28 counts; (4) Ne IX, 93 counts; (5) Fe XVIII, 23 counts; and (6) second Fe XVII maps, 145 counts.

TABLE 1

FCS LINE PROFILE OBSERVATIONS

Ion	λ (Å)	Time (UT)	Transition	I (ergs cm^{-2} s^{-1} sr^{-1})
Fe XVII	15.01	18:06	$2p^6\ ^1S_0$–$2p^5 3d\ ^1P_1$	3971 ± 238
Fe XVII	15.26	18:06	$2p^6\ ^1S_0$–$2p^5 3d\ ^3D_1$	2092 ± 188
O VIII	18.97	18:13	$1s^2 S_{1/2}$–$2p^2 P_{3/2}$	8507 ± 1531
Mg XI	9.17	18:13	$1s^2\ ^1S_0$–$1s2p\ ^1P_1$	233 ± 72
Ne IX	13.44	18:21	$1s^2\ ^1S_0$–$1s2p\ ^1P_1$	1223 ± 183
Fe XVIII	14.203	18:24	$2p^5\ ^2P_{3/2}$–$2p^4 3d\ ^2D_{5/2}$	571 ± 257
	14.215		$2p^5\ ^2P_{3/2}$–$2p^4 3d\ ^2P_{3/2}$	

each fit with two Voigtian line profiles, and the measured flux is the total flux of the two lines. These line fits are discussed in more detail by Waljeski (1992). The line intensities at the Sun derived from the FCS line profile measurements are listed in Table 1.

2.2. *Broadband Images*

The AS&E High Resolution Imaging Sounding-Rocket Payload was launched on a sounding rocket from White Sands Missile Range. The AS&E playload was first described by Vaiana, Krieger, & Timothy (1973). A more recent description is given by Moses, Krieger, & Davis (1986). The payload contains a fused-quartz grazing-incidence telescope mirror, five interchangeable filters (a white-light filter, two beyllium soft X-ray filters, and two aluminized-polypropylene soft X-ray filters), and photographic film camera. Full-disk images of the Sun on Kodak SO-212 film were obtained for a variety of exposure times, ranging from 0.25 s to 60 s, between 18:19:28 UT and 18:26:38 UT. The entire sequence of observations and the properties of each of the filters for this flight are described by Waljeski (1992). Two images were selected for this analysis: a 3 s exposure through a polypropylene filter, taken starting at 18:17:08 UT, and a 30 s exposure through a beryllium filter, taken starting at 18:17:17 UT (see Table 2).

2.2.1. *Film Calibration*

The film calibration techniques are discussed in detail in the doctoral thesis of Waljeski (1992). The film was handled and developed as described by Moses et al. (1989). The images were digitized with a step size of 2.″85 × 2.″85. The film calibration is necessarily an iterative process, because the film response is wavelength dependent and the incident-filter X-ray spectrum depends on the temperature and composition of the observed plasma. The shape of the film characteristic curve was found by comparing the photographic densities of images with different exposure times, as described by Moses et al. (1989). This relative calibration technique is based on the histogram calibration method of Cook, Ewing, & Sutton (1987). The film speed (the absolute calibration) is derived from laboratory film response measurements at two wavelengths (8 Å and 44 Å) by the iterative method described by Vaiana et al. (1977) and Webb & Davis (1985).

TABLE 2

AS&E SOUNDING-ROCKET PAYLOAD OBSERVATIONS

Filter	Time (UT)	Exposure Time (s)	Waveband (Å)
Aluminized polypropylene	18:17:08	3	8–39, 44–60
Beryllium	18:17:17	30	8–29

2.2.2. *Alignment of the Broadband Images with the FCS Observations*

The AS&E broadband images and the FCS observations were aligned by comparing the white-light images from each instrument to find the position of the solar limb. There are no sunspots visible on the *SMM* white-light image, so the rotational orientation was fixed by comparing the morphology of the broadband images and the first FCS Fe XVII map, which is the largest and the brightest of the complete FCS maps from this orbit. Figure 2 shows the aligned polypropylene-filtered image and Fe XVII map, with the 30″ × 30″ area of the FCS line profile measurements indicated on each image. The accuracy of this alignment is estimated to be ±10″ (which is ±3 pixels of the broadband image or ±1 pixel of the FCS map).

2.2.3. *Compensation for the Effects of Scattering*

The point response of the AS&E grazing-incidence telescope is sharply peaked with a full width at half-maximum of about 2.″5. The wings of the point response function are broad, because scattering by the telescope surfaces deposits some of the incident flux far from the source position. The response of the AS&E soft X-ray grazing-incidence telescope and film is discussed in detail by Moses et al. (1986).

A simple scattering correction is made for this data set, as described by Waljeski (1992). The effect of the point response of the telescope mirror is to scatter the incident energy from the coronal sources in the area of observation to points on the film outside this area and to scatter energy from coronal sources outside the area of observation to inside the area on the film. An estimate of the effect of scattering is made by assuming a source distribution for a 356″ × 356″ area and calculating the energy scattered into and out of the 30″ × 30″ area corresponding to the area of the FCS line profiles. The actual source function is not known, but since the point response function of the mirror is sharply peaked (if broadly winged), the observed image approximates the source. The ratio of the final brightness in the central area after scattering to the source brightness of that area is an estimate of the factor by which the observed broadband flux in the area of interest must be changed to compensate for the effects of scattering.

2.2.4. *Selection of the Area of Interest*

To make the intensities measured by the FCS line profiles and AS&E broadband images comparable, the broadband images are averaged, weighted by the FCS field of view. This weighted total broadband flux is then corrected for scattering. The polypropylene-filtered flux in the region of interest is corrected for point spread by a multiplicative factor of 1.87, and the beryllium-filtered flux is corrected by a factor of 1.91 (Waljeski 1992).

The principal sources of uncertainty in the broadband inten-

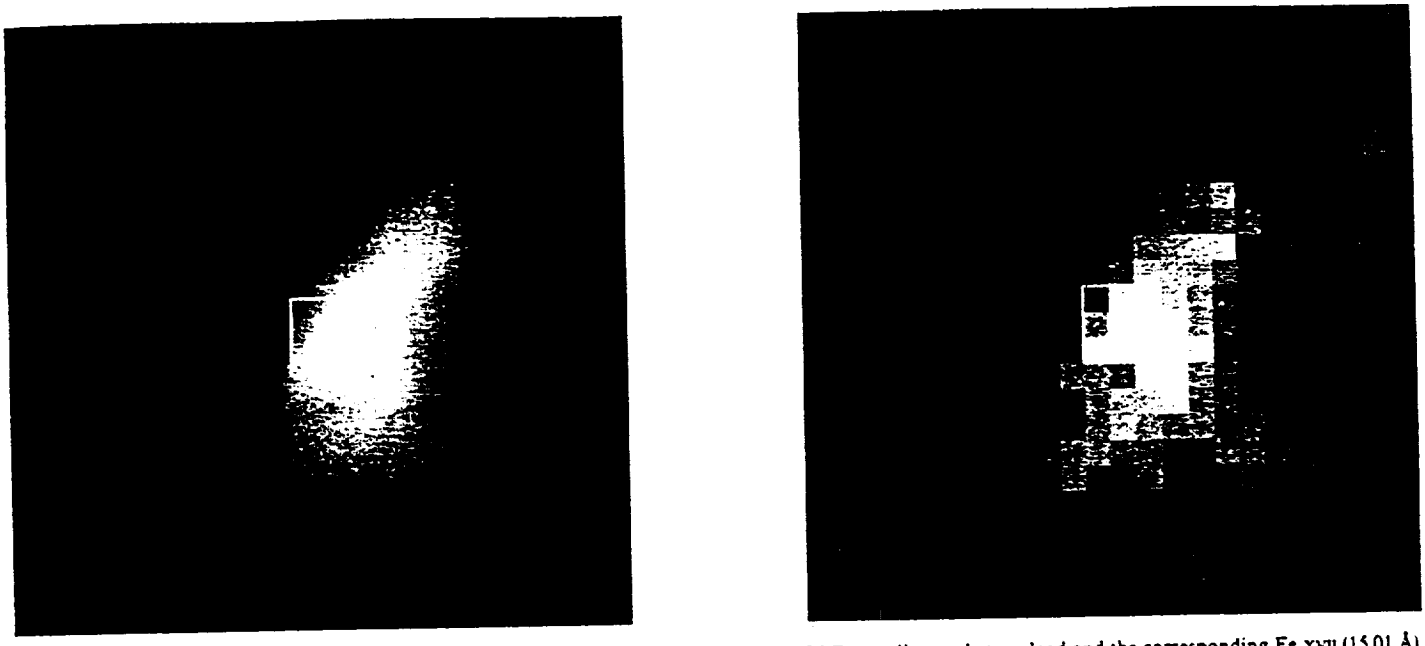

FIG. 2.—Polypropylene-filtered soft X-ray image (8–39, 44–60 Å) of AR 4901 from the AS&E sounding-rocket payload and the corresponding Fe XVII (15.01 Å) map from the FCS. Each image is 4′ on a side. The 30″ × 30″ area corresponding to the field of view over which the FCS line profile scans were made is marked on each image by the superimposed boxes. The broadband X-ray image presented here has been digitized and smoothed to approximate the FCS resolution.

sity measurements are the film calibration, the alignment with the FCS observing area, and the compensation for scattering. The total uncertainty in the broadband filtered spectra is estimated to be about ±50%.

3. PLASMA DIAGNOSTICS

3.1. *Temperature and Emission Measure from FCS Lines*

For nearly optically thin emission from an isothermal plasma, the intensity emitted at the Sun, $I_i(\lambda)$ (ergs cm^{-2} s^{-1} sr^{-1}), in a soft X-ray emission line i at wavelength λ_i is related to the plasma properties of the corona by the expression

$$I_i(\lambda) = P\epsilon_i(T)\int n_e^2\, dl\,, \qquad (1)$$

where P is the photon escape probability, $\epsilon_i(T)$ is the emissivity of the line (the intensity emitted per unit emission measure at temperature T), n_e is the electron density, l is the distance along the line of sight, and $\int n_e^2\, dl$ is the emission measure. For an escape probability of unity, this expression reduces to the optically thin case.

3.1.1. *Emissivity Calculations*

The following expression is used to calculate the emissivity of each line:

$$\epsilon_i(T) = \frac{hc}{4\pi\lambda_0}\left[\frac{8.63\times10^{-6}}{T^{1.2}}\frac{\langle\Omega\rangle B}{g}\exp\left(\frac{-\Delta E}{kT}\right)\right]\frac{n_i}{n_{el}}\frac{n_{el}}{n_H}\frac{n_H}{n_e}\,, \qquad (2)$$

where λ_0 is the wavelength at line center, T is the electron temperature, $\langle\Omega\rangle$ is the Maxwellian-averaged collision strength, B is the branching ratio, g is the statistical weight of the lower level, ΔE is the energy difference between the upper and lower levels, n_i/n_{el} is the ionization fraction, n_{el}/n_H is the abundance of the emitting element relative to hydrogen, n_H/n_e is the ratio of the number densities of hydrogen and electrons ($n_H/n_e = 0.8$), h is Planck's constant, c is the speed of light, and k is Boltzmann's constant.

The most recent atomic physics calculations available are included in the emissivities of the FCS lines. The wavelengths, collision strengths, branching ratios, and statistical weights of

TABLE 3

ATOMIC PARAMETERS FOR FCS LINES

Ion	λ(Å)	$\langle\Omega\rangle$	B	g	$\langle\Omega\rangle B/g$	f_{ik}	References
Fe XVII	15.01	0.115	1.000	1	0.115	2.479	1, 2, 3
Fe XVII	15.26	0.029	1.000	1	0.029	0.600	1, 2, 3
O VIII	18.97	0.051	1.000	2	0.026	0.416	4, 5
Mg XI	9.17	0.017	1.000	1	0.017	0.745	5, 6, 7, 8
Ne IX	13.445	0.023	1.000	1	0.023	0.723	5, 6, 7, 8
Fe XVIII ($^2D_{5/2}$)	14.203	0.180	0.874	4	0.067	0.994	9, 10, 11
Fe XVIII ($^2P_{3/2}$)	14.215	0.113	1.000	4		0.636	

REFERENCES.—(1) Bhatia & Doschek 1992; (2) Zhang & Sampson 1989; (3) Hagelstein & Jung 1987; (4) Abu-Salbi & Callaway 1981; (5) Wiese, Smith, & Glennon 1966; (6) Kato & Nagazaki 1989; (7) Zhang & Sampson 1987; (8) Wiese, Smith, & Miles 1969; (9) Cornille et al. 1992; (10) Sampson, Zhang, & Fontes 1991; (11) Fawcett 1984.

TABLE 4

ELEMENTAL ABUNDANCES

	Photospheric (Grevesse & Anders 1991)	Adopted Coronal (Meyer 1985b)	Coronal
H	12.00	12.00	12.00 ± 0.73
O	8.93	8.39	9.30
Ne	8.07	7.54	8.45
Mg	7.58	5.57	8.48
Fe	7.51*	7.59	8.50

NOTE.—Values listed are log of abundance relative to the log abundance of H = 12.00.

* The photospheric Fe abundance is the more recently determined value from the review by Grevesse et al. 1992.

the lower levels of each transition are listed in Table 3. The single value of $\Omega B_i g$ listed in Table 3 is the value for the sum of the two Fe XVIII lines.

The Maxwellian-averaged collision strength listed in Table 3, $\langle\Omega\rangle$, is the collision strength as a function of energy, integrated over the electron energies corresponding to a Maxwellian distribution of velocities. The averaged collision strengths are calculated for the velocity distribution of the temperature at the maximum emissivity of each line. To be most accurate, the Maxwellian-averaged collision strength should be calculated as a function of temperature, but this approximation does not significantly affect the calculated emissivities in this case.

The emissivities of the six FCS lines are calculated from equation (2) with each of the sets of elemental abundances listed in Table 4, the atomic data listed in Table 3, and the ionization fractions of Arnaud & Rothenflug (1985). The reasons for choosing these ionization fractions are explained in detail in § 5.6. The emissivities for the adopted coronal abundances of Meyer (1985b) are plotted in Figure 3.

3.1.2. *Optical Depth*

The photon escape probability, P, is included in equation (1) to account for optical depth due to resonance scattering. We assume that the effect of resonance scattering is only to scatter photons out of the line of sight. This assumption is reasonable for small optical depths and for the geometry of the observed area; since the center of the active region is bright relative to the surrounding areas of the corona, the flux scattered out of the region of interest should be much greater than the flux scattered in. We also assume that the emissivity of the plasma is constant along the line of sight in the corona and that the line profile shape is Gaussian. In this approximation, the photon escape probability is

$$P(\tau_0) = \int \frac{1 - \exp(-\tau_0 \phi)}{\sqrt{2\pi}\sigma\tau_0}\, d\lambda\,, \tag{3}$$

where τ_0 is the optical depth at line center and ϕ is the Gaussian line profile:

$$\phi = \exp\left[-\frac{(\lambda - \lambda_0)^2}{2\sigma^2}\right]. \tag{4}$$

The optical depth at line center, τ_0, resulting from resonance scattering is given by the expression

$$\tau_0 = \left(\frac{\pi e^2}{mc^2}\right)\lambda_0^2 f_{lu} \frac{n_i}{n_{el}} \frac{n_{el}}{n_H} \frac{n_H}{n_e} \left(\frac{1}{\sqrt{2\pi}\sigma}\right) \int n_e\, dl\,, \tag{5}$$

where λ_0 is the wavelength of line center and f_{lu} is the absorption oscillator strength of the transition from the lower level l to the upper level u. The constants e, m, and c are the electron charge, the mass of the proton, and the speed of light, respectively. The line width, σ, is related to the plasma properties by the expression

$$\sigma^2 = \frac{\lambda_0^2}{2c^2}\left(\frac{2kT}{M} + v_{nt}^2\right), \tag{6}$$

where M is the atomic mass of the ion and v_{nt} is the nonthermal velocity of the plasma. The nonthermal velocity is assumed to be 20 km s^{-1} for this analysis. The reasons for assuming this value of nonthermal velocity are discussed in § 5.7. The effect of the nonthermal velocity assumption on the final results of our analysis are also discussed in § 5.7.

The intensity ratio of the two Fe XVII lines, which have significantly different oscillator strengths, is a sensitive indicator of the optical depth. Combining equation (1) and equation (2) shows that the ratio of the fluxes of two lines produced by the same ion is independent of abundance and ionization fraction and only weakly temperature dependent. For an optically thin plasma, the predicted intensity ratio of the two Fe XVII lines (the 15.01 Å line to the 15.26 Å line) is 3.80, the ratio of the emissivities. The observed Fe XVII ratio was 1.90 ± 0.21, a factor of 2 lower than expected for the optically thin case, indicating that the photon escape probability is not unity.

The Fe XVII ratio, calculated as a function of the optical depth at line center of the 15.01 Å line, is plotted in Figure 4. The oscillator strengths used in this calculation, f(15.01 Å) = 2.479 and f(15.26 Å) = 0.600, are from Bhatia & Doschek (1992). The observed Fe XVII ratio is marked on the curve, indicating that the optical depth of the 15.01 Å line is 4.2 (+1.3, −1.0).

Once the opacity of one line is known, the optical depths of all the lines can be calculated. If we assume the Fe XVII ionization fraction and the abundance of iron relative to hydrogen, the only unknown quantity in the expression for the optical depth at line center, given by equation (5), is the column

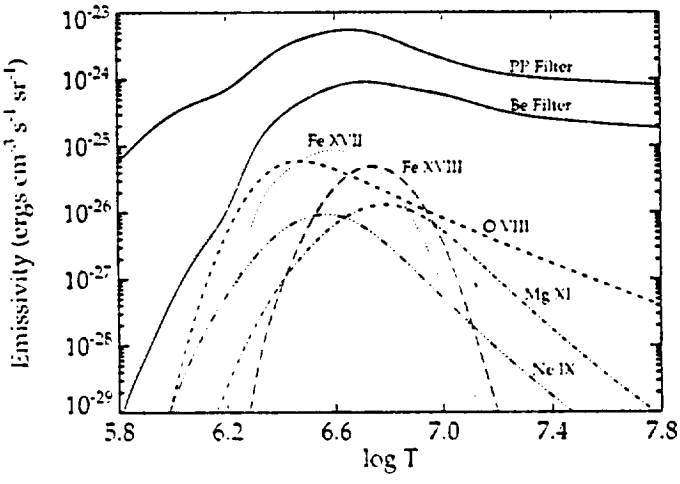

FIG. 3.—Emissivities of the lines observed by the *SMM* FCS, calculated from equation (2), with the collision strengths from Table 3 and the ionization fractions from Arnaud & Rothenflug (1985). The Fe XVII emissivity plotted is that of the line at 15.01 Å. The emissivity of the Fe XVII line at 15.26 Å has an almost identical shape, with slightly lower emissivity values. The broadband filtered spectrum integrals for the polypropylene and beryllium filters are superimposed on the plot for comparison of temperature sensitivity. The filtered spectrum integral has units of ergs cm^{-2} s^{-1}.

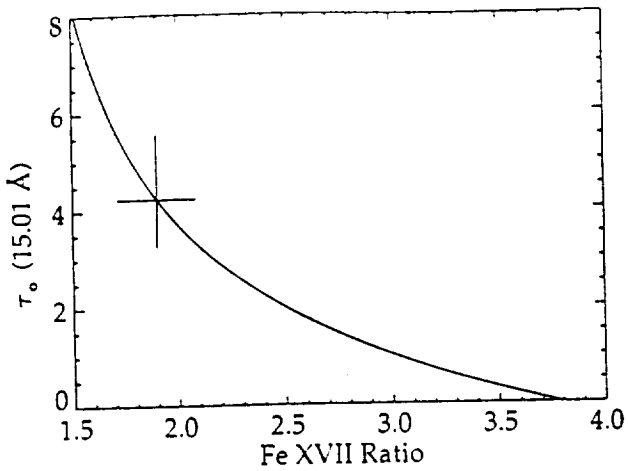

FIG. 4.—Optical depth at line center of the 15.01 Å Fe XVII line plotted as a function of the intensity ratio of the two Fe XVII lines, I (15.01 Å)/I (15.26 Å). The measured value of the Fe XVII ratio and the corresponding optical depth are indicated. The observed Fe XVII intensity ratio is 1.90 ± 0.21, which implies that $\tau_0(\lambda = 15.01\ \text{Å}) = 4.24\ (+1.3, -1.0)$.

density, $\int n_H\, dl$. The optical depth of the 15.01 Å line implies the $\int n_e\, dl = 1.05 \times 10^{20}$ cm^{-2} for this region, assuming the adopted coronal iron abundance (Meyer 1985b) and $\int n_e\, dl = 1.28 \times 10^{20}$ cm^{-2} for the photospheric iron abundance (Grevesse et al. 1992). Using these values and the oscillator strengths listed in Table 3, the optical depths at line center of all the observed lines are calculated and listed in Table 5, for both the photospheric abundances and the adopted coronal abundances.

The photon escape probabilities for each of the lines are calculated by means of equation (3) and are also listed in Table 5. For the Fe XVII line at 15.01 Å with an optical depth of 4.24, the escape probability is 0.358. For this active region, the effect of optical depth is significant compared with the uncertainties in the intensity measurements for both of the Fe XVII lines, the O VIII line, and the Ne IX line.

Resonance scattering of Fe XVII was also examined for these same FCS line data by Schmelz et al. (1992), who found an optical depth of 2.4 (+0.3, −0.4) for the Fe XVII line at 15.01 Å. These authors compared the line ratio of Fe XVII (15.01 Å)/O VIII (18.97 Å) to ratios of other FCS lines involving O VIII, Ne IX, Mg XI, and Fe XVIII, under the assumption that only the Fe XVII line at 15.01 Å is significantly affected by resonance scattering. This method underestimates the magnitude of the effect if the O VIII line is also significantly affected, as shown here. The present study, which compares two affected Fe XVII lines to obtain a more direct, abundance-independent measure of the resonance scattering, provides a more self-consistent treatment of the scattering opacity of all the lines, both in the calculation of optical depths and in the determination of plasma parameters.

3.2. *Temperature and Emission Measure from Broadband Images*

For an isothermal optically thin plasma, the intensity F_i, in ergs cm^{-2} s^{-1}, incident on the film at the focal plane of the broadband telescope, through a given filter, i is related to the temperature, emission measure, and composition of the emitting coronal plasma by the equation

$$F_i = \frac{A}{4\pi f^2} \int p(\lambda, T)\eta_i(\lambda)d\lambda \int n_e^2\, dl\,, \qquad (7)$$

where A is the geometrical collecting area of the telescope, f is the telescope focal length, $\eta_i(\lambda)$ is the product of the filter transmission and the telescope reflectivity as a function of wavelength, and $p(\lambda, T)$ is the power emitted at wavelength λ at temperature T, per unit emission measure.

3.2.1. *The Broadband Filtered Spectra*

For an isothermal plasma, the integral over wavelength in equation (7) (the filtered spectrum integral), expresses the temperature dependence of the flux equation. The calculation of the filtered spectrum integrals is described in detail by Waljeski (1992).

The solar spectrum, $p(\lambda, T)$, is calculated between 8 and 60 Å using a program written by Lemen (1990). In this wavelength range, both continuum emission and a large number of emission lines (about 500) produced by many different elements and ionization species contribute to the solar spectrum. Lemen's program generates a model solar spectrum using the line emissivities of Mewe, Gronenschild, & van den Oord (1985) and a model of the solar soft X-ray continuum. The emissivities tabulated by Mewe et al. (1985) are not the most recent calculations for many of the lines, but they are in a form that is convenient for the broadband data analysis and are sufficiently accurate for this purpose, considering the large number of lines that contribute to each of the broadband filtered spectra.

The relative contributions of lines produced by all ions of Ne, O, Mg, and Fe to the filtered solar spectra are plotted in Figures 5*a* and 5*b* for the adopted coronal abundances of Meyer (1985b). The percentage contribution of the continuum emission is also plotted. This plot shows that the filtered spectra are dominated by line emission, particularly from iron ions, at active-region temperatures, about 2×10^6 K to 3×10^6 K. The percentage contribution of iron lines to the filtered spectra is about 80%, and the percentage contribution of the continuum is less than 20%, over most of this temperature rage.

TABLE 5

OPTICAL DEPTHS AND PHOTON ESCAPE PROBABILITIES

Ion	λ_0 (Å)	Photospheric Abundances		Adopted Coronal Abundances	
		τ_0	P	τ_0	P
Fe XVII	15.01	4.24	0.358	4.24	0.358
Fe XVII	15.26	1.04	0.716	1.04	0.716
O VIII	18.97	7.59	0.233	1.82	0.581
Mg XI	9.17	0.80	0.770	0.65	0.806
Ne IX	13.44	2.79	0.466	0.69	0.797
Fe XVIII	14.21	0.20	0.932	0.20	0.932

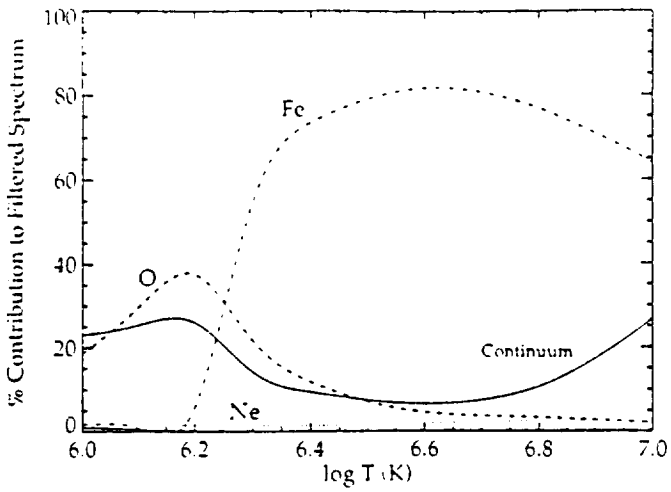

FIG. 5a

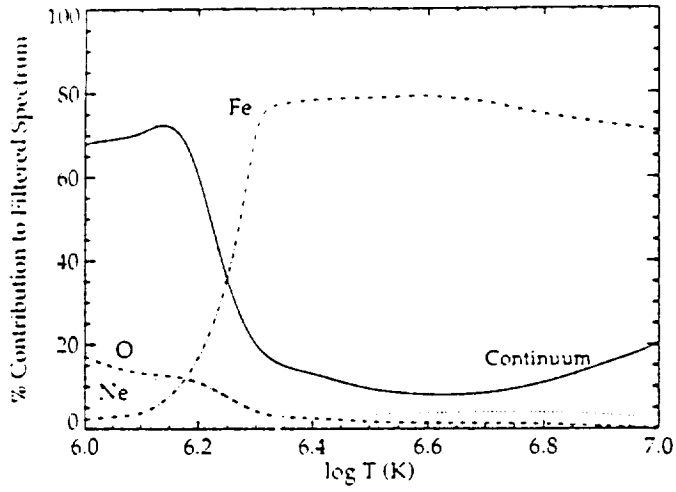

FIG. 5b

FIG. 5.—Percentage contribution of all the lines of Fe, O, and Ne and of the continuum, to the filtered solar spectra. The contributions of lines of Mg to the filtered spectra are less than 1% for most temperatures, and so are not plotted. (*a*) Percentage contributions of each element to the aluminized-polypropylene-filtered soft X-ray spectrum (8–39, 44–60 Å); and (*b*) Percentage contributions to the beryllium-filtered soft X-ray spectrum (8–29 Å). For both filters, the Fe lines dominate the filtered spectrum over a large range of temperatures, making up about 80% of the total flux through each filter at temperatures characteristic of quiet coronal active regions (about 3×10^6 K). The total contribution of all the elements is not equal to 100% at all temperatures because other elements, including C, Ca, Ni, N, and S, also contribute to the filtered solar spectra in this temperature range.

The broadband spectrum is assumed to be optically thin. This assumption is made because it is impractical to calculate the optical depth and photon escape probability for each of the more than 500 lines that contribute to the filtered spectra, and because this assumption is not likely to have a significant effect on the integrated filtered flux (relative to the 50% uncertainty in the broadband intensity measurement). Only the brightest lines are likely to have large optical depths in this case, so most of the lines that contribute to the broadband spectrum should not be significantly affected by resonance scattering.

The filtered spectrum integrals for the polypropylene and beryllium filters are superimposed on the line emissivity plot (Figure 3) for comparison of the temperature responses. The units of the filtered spectrum integrals (ergs cm^{-2} s^{-1}) are not the same as the units of the line emissivities (ergs cm^{-3} s^{-1} sr^{-1}) because the waveband is selected by the telescope reflectivity and the filter responses, so the broadband instrumental response can not be separated from the emissivity of the passband (Waljwski 1992).

4. RESULTS

The relative abundances of iron, oxygen, magnesium, and neon in the corona are determined by finding a model active-region plasma with a temperature, emission measure, and elemental composition that would produce the observed line and broadband intensities. We then use the additional information provided by the optical depths of the Fe XVII lines and the geometry of the region as a diagnostic of absolute abundance.

4.1. *Relative Abundances of* Fe, O, Mg, *and* Ne

We first consider the simplest temperature and emission measure distribution: the isothermal model. If the observed active region is composed of isothermal plasma, then it should be described by a single temperature and emission measure. The emission measure, $\mathrm{EM}(T) = \int n_e^2\, dl$, necessary for a plasma of a given temperature and composition to produce the observed flux is found by inverting the intensity equations (for FCS lines, eq. [1], and for broadband intensities, eq. [7]). The derived emission measures are plotted as a function of the assumed isothermal temperature in Figure 6*a* for the photospheric abundances of Grevesse & Anders (1991) and in Figure 7a for the adopted coronal abundances of Meyer (1985b). These plots provide a qualitative indication of how well the isothermal model plasma fit the observed intensities.

A quantitative measure of the consistency of the observed intensities with the plasma model is provided by the reduced χ^2 of the expected intensities for each temperature and emission measure:

$$\chi^2(T, \mathrm{EM}) = \frac{1}{N-1} \sum_{i=1}^{N} \left[\frac{I_i - I_i'(T, \mathrm{EM})}{\sigma_i} \right]^2, \qquad (8)$$

where $N - 1$ is the number of degrees of freedom (i.e., the number of observations minus one), I_i is the observed intensity, $I_i'(T, \mathrm{EM})$ is the intensity predicted from an isothermal model plasma with temperature T and emission measure EM, and σ_i is the standard deviation of each observed intensity.

The temperatures of isothermal plasmas consistent with the observations are found by the following method: The reduced χ^2 (T, EM) is calculated for model isothermal plasmas with a range of temperatures (1×10^6 K to 10×10^6 K). At each temperature, we find the model plasma that best reproduces the observed intensities, by identifying the emission measure that yields the minimum value of χ^2 (T, EM) at that temperature. A minimum reduced $\chi_0^2(T)$ of unity or less indicates that an isothermal plasma with the given temperature is consistent with the observations for some emission measure or range of emission measures.

4.1.1. *Photospheric Abundances*

In Figure 6*a*, we have plotted the emission measures derived for each line and broadband intensity measurement as a function of the assumed temperature for a model plasma having photospheric abundances (Table 4). On this plot, the emission measures determined from all the line and broadband observations do not appear to be mutually consistent for an isothermal plasma of any temperature. The FCS lines from two clusters on

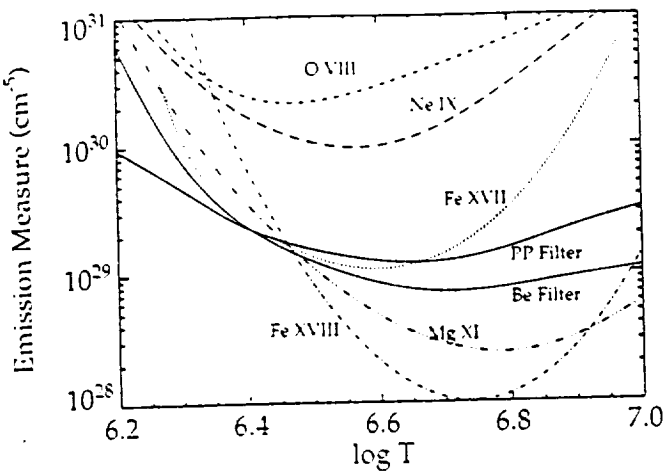

FIG. 6a

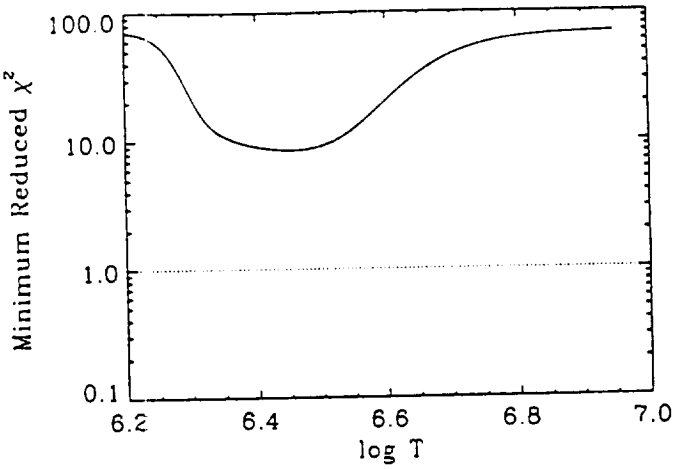

FIG. 6b

FIG. 6.—(*a*) Emission measure as a function of temperature from the joint observations, assuming the photospheric relative abundances and an isothermal emitting region. Each curve represents the emission measure derived from a measured line or broadband intensity, as a function of the assumed temperature. The emission measure is calculated from equation (1) for the FCS line intensities and from equation (7) for the broadband intensities. (*b*) Minimum (with respect to emission measure) reduced χ^2 of the intensities predicted from an isothermal plasma with photospheric abundances, as a function of temperature. The minimum reduced χ^2 is significantly greater than unity for the entire temperature range, indicating that the observed line and broadband intensities are not consistent with the emission from an isothermal photospheric plasma.

the temperature-emission measure plot: one cluster near the emission measure determined by the broadband polypropylene-filtered spectrum, and another cluster at an emission measure about an order of magnitude higher. The group with lower emission measure includes the lines of Fe XVII, Fe XVIII, and Mg XI, all low-FIP elements, as well as the broadband filtered spectra. As shown in Figures 5*a* and 5*b*, the broadband filtered spectra are dominated by emission lines of iron, which is a low-FIP element. The higher emission measure group contain the lines of O VII and Ne IX, both high-FIP elements. The separation of the emission measures determined from the lines of high-FIP and low-FIP elements for the photospheric abundances suggests the fractionation of the composition of the solar corona with FIP discussed by Meyer (1985b).

The minimum reduced χ^2 of the intensities, plotted in Figure 6*b*, is not less than 8.5 for any temperature. Therefore, the probability that the joint line and broadband observations are consistent with an isothermal plasma of photospheric composition for any temperature or emission measure is less than 0.1% (Bevington 1969).

4.1.2. *Adopted Coronal Abundances*

The emission measures derived from all of the observed intensities are plotted in Figure 7*a* for an isothermal plasma with the FIP-fractionated adopted coronal abundances of

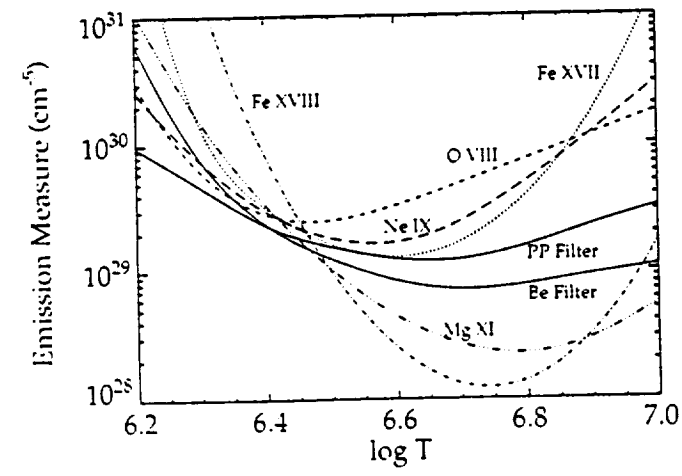

FIG. 7a

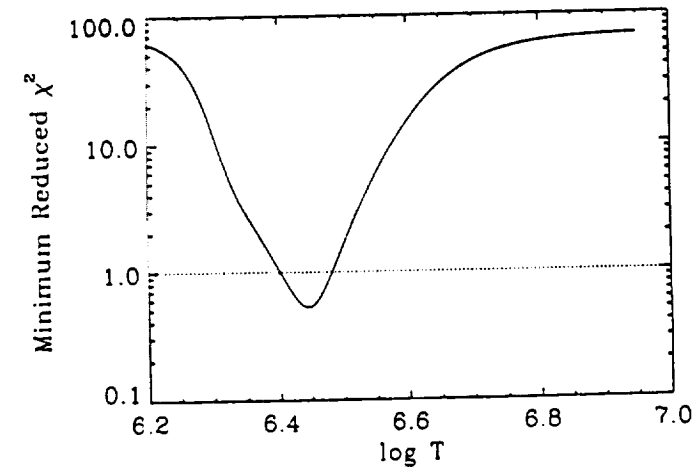

FIG. 7b

FIG. 7.—(*a*) Emission measure as a function of temperature, assuming the FIP-biased adopted coronal abundances (Meyer 1985b) and an isothermal emission measure distribution. Each curve represents the emission measure derived from a measured line or broadband intensity, as a function of the assumed temperature. The emission measure is calculated from equation (1) for the FCS line intensities and from equation (7) for the broadband intensities. (*b*) Minimum reduced χ^2 of the line and broadband intensities predicted for an isothermal plasma with the adopted coronal abundances of (Meyer 1985b), as a function of temperature. The value of χ^2_0 is less than or equal to unity between 2.5×10^6 K and 3.0×10^6 K, indicating that the observed intensities are consistent, for any temperature in this range, with the emission from an isothermal plasma having the adopted coronal relative elemental abundances

Meyer (1985b). On this plot, the emission measures determined by the joint observations seem to be consistent with one another for active-region temperatures (between 2×10^6 K and 3×10^6 K).

The minimum reduced chi-squared of the intensities, plotted in Figure 7*b*, is less than one over a range of temperatures from 2.5×10^6 K to 3.0×10^6 K, indicating that these data are consistent with an isothermal plasma of adopted coronal composition, having any temperature in this range. The range of values of emission measure corresponding to this temperature range were 3.0×10^{29} cm^{-5} to 1.7×10^{29} cm^{-5}. The minimum value of $\chi^2_0(T)$ corresponds to a probability of fit of 90% (Bevington 1969) for an isothermal plasma with a temperature of 2.8×10^6 K and an emission measure of 2.3×10^{29} cm^{-5}.

4.2. *Absolute Abundances*

We have confirmed, assuming an isothermal plasma, that the ratio of the abundances of the high-FIP elements (O and Ne) to the low-FIP elements (Mg and Fe) is about a factor of 3.5 less in the corona than in the photosphere. The additional information provided by the optical depths of the Fe XVII lines and the geometry of the region makes it possible to constrain the abundances of the heavier elements relative to the abundance of hydrogen, as well as to determine the electron density.

Assuming that the plasma is uniformly distributed along the line of sight through the active region, the active-region density and path length can be determined from the emission measure, $\int n_e^2\, dl$, and the line-of-sight integral of density, $\int n_e\, dl$, using the relations

$$n_e = \frac{\int n_e^2\, dl}{\int n_e\, dl} \tag{9}$$

and

$$\Delta l = \frac{\int n_e\, dl}{n_e}\,. \tag{10}$$

The abundance of iron relative to hydrogen may then be determined by comparing the path length calculated from the optical depth of the Fe XVII line to the geometry of the active region seen in the broadband images. Examining equation (5), we see that the expected path length is inversely proportional to the absolute abundance of iron, n_{Fe}/n_H. We assume that all the parameters in the equation, including the ionization equilibrium and the atomic parameters are known. Therefore, it is possible to determine the absolute abundance of iron, n_{Fe}/n_H, given the measured optical depth and the path length.

4.2.1. *Density and Path Length for Meyer Abundances*

The active-region density and path length are first calculated for the adopted coronal abundances of Meyer (1985b). The value of the integral of density along the line of sight derived from the ratio of the two Fe XVII lines, $\int n_e\, dl = 1.05 \times 10^{20}$ cm, and the emission measure derived from the observed intensities, $\int n_e^2\, dl = 23 \times 10^{29}$ cm^{-2} ($+0.8 \times 10^{29}$ cm^{-2}, -0.4×10^{29} cm^{-2}) give a density, $n_e = 2.2 \times 10^9$ cm^{-3} ($+0.8 \times 10^9$ cm^{-3}, -0.4×10^9 cm^{-3}). This density is in reasonable agreement with densities derived from density-sensitive lines of Fe XII, Fe XIII, Fe XIV, and Fe XV (Dere 1982).

The path length obtained for these abundances is 4.7×10^{10} cm (-1.8, $+0.9$) or 653″ (-281″, $+228$″). This path length is much longer than could be expected for this region. The broadband image in Figure 2 shows that the emission from the entire active region spans only about 150″, while the calculated path length is about a third of the diameter of the Sun. It is difficult to see how such a long path length could be associated with this active region. This active region is near the limb of the Sun (at about 70° west), but the 30″ × 30″ area of interest is entirely on the disk in this line of sight, so material from the other side of the limb could not be extending the path length.

The path length along the line of sight cannot be measured directly from the broadband or the FCS images, but a reasonable estimate may be made by measuring the characteristic lengths of the region. The largest dimension (a southeast-to-northwest diagonal) of the entire active region is about 150″. The characteristic path length is estimated from profiles through the area of interest, made approximately east to west across the maps of $\int n_e^2\, dl$ and $(\int n_e^2\, dl)^{1/2}$ constructed from the broadband images. From the measured full width at half-maximum of these profiles, we estimate that the path length is 80″ ± 40″.

4.2.2. *Determination of Absolute Abundances*

The path length of 653″ derived using the adopted coronal abundance of Fe (Meyer 1985b) is clearly inconsistent with the observed dimensions of this active region. The derived and observed path lengths can be made consistent if we take hydrogen to behave as a high-FIP element, as suggested recently by Meyer (1993a, 1993b). In order to account for the observed path length, the abundance of iron relative to hydrogen must be 3.20×10^{-4} (-2.12×10^{-4}, $+2.00 \times 10^{-4}$). This iron abundance is higher than the value given by Meyer (1985b) by a factor of 8.2 (-5.4, $+5.0$).

The calculated temperature, electron density, optical depth, and escape probability are not affected by this change in the assumed value of the hydrogen abundance, while the emission measure, and the column density are inversely proportional to n_{Fe}/n_H. For the absolute abundances determined here, $\int n_e^2\, dl = 2.8 \times 10^{28}$ and $\int n_e\, dl = 1.3 \times 10^{19}$.

Since the relative abundances of Fe, O, Mg, and Ne given by Meyer (1985b) are consistent with these observations, we are able to calculate the abundances of O, Mg, and Ne relative to hydrogen, given the calculated value of n_{Fe}/n_H. These absolute abundance values are listed in the last column of Table 4.

If we assume that all the relative abundances of the heavier elements given by Meyer (1985b) for the solar corona are correct, a complete set of coronal abundances that is consistent with the present results can be obtained. These new coronal abundances, listed in Table 6, are calculated by increasing the Meyer (1985b) adopted coronal abundances of all the elements except hydrogen by a factor of 8.2.

The uncertainty in the hydrogen abundance listed in Tables 5 and 6 results from the measurement of the Fe XVII intensities and the path length. The simplicity of our analytical models, which assume homogeneous conditions along the line of sight, may contribute systematic errors, in addition to the stated measurement errors, if the material along the line of sight is not uniformly distributed.

4.2.3. *The Effect of Inhomogeneous Density*

To calculate the absolute abundances, we assumed a uniform density distribution in deriving the path length, Δl, from equations (9) and (10). In this section, we consider the effect of assuming an inhomogeneous density distribution on the expected path lengths and abundances.

TABLE 6

CORONAL ABUNDANCES

Element	Abundance
H	12.00 ± 0.73
He	11.90
C	9.28
N	8.50
O	9.30
Ne	8.45
Na	7.35
Mg	8.48
Al	7.35
Si	8.50
S	7.84
Ar	7.24
Ca	7.38
Fe	8.50
Ni	7.24

NOTE.—Values listed are log of abundance normalized so that the log abundance of H = 12.00. The university listed is the uncertainty in the abundance of the heavier elements relative to the abundance of H.

Two reasonable models of nonuniform density are considered: a hydrostatic model and a filamentary model (Fig. 8). These models are functions of a characteristic length h and density n_0. The hydrostatic distribution reproduces the decline in intensity with height observed in the broadband X-ray image. In the hydrostatic model, h is the scale height of the distribution. The filamentary model has a filling factor of $\frac{1}{2}$, and approximates the looplike structure of active regions.

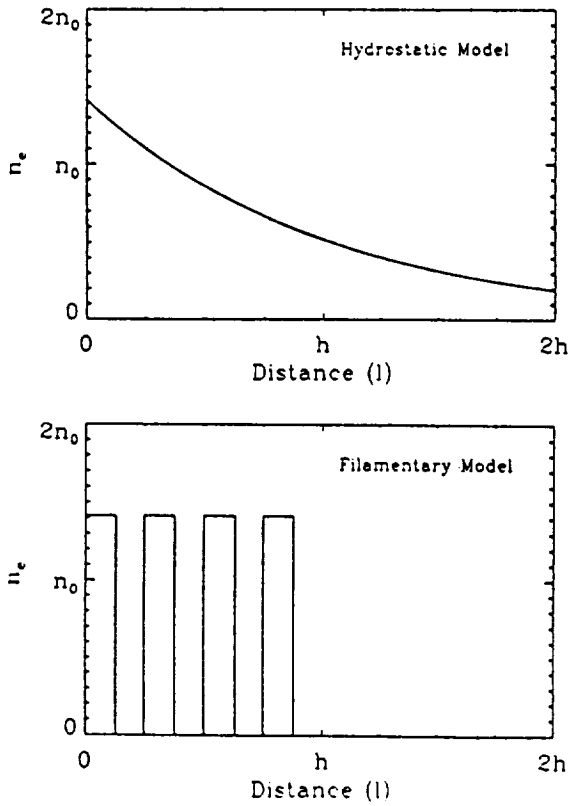

FIG. 8.—Two inhomogeneous density distributions characteristic of active regions. These models are functions of a characteristic length h and density n_0 and are scaled so that the emission measure is equal to $n_0^2 h$.

Each density distribution is scaled so that the emission measure is equal to $n_0^2 h$.

For the hydrostatic model, the path length Δl calculated from equations (9) and (10) equal to $2h$. Consequently, if we had assumed a uniform density distribution with a characteristic length h, we would have underestimated the path length by a factor of 2 and thus overestimated the abundance of iron relative to hydrogen by a factor of 2. For the filamentary model, the effect of nonuniform density on the absolute abundances works in the opposite sense: For a filling factor of $\frac{1}{2}$, the calculated path length is $h/2$, so if a uniform density were used, the path length would be overestimated and the iron abundance underestimated by a factor of 2. The actual density distribution in this active region is probably some combination of a gradually decreasing density with looplike structures, and the effects of the two density distributions on the derived abundances would tend to cancel.

4.3. *Interpretation of the Results*

We have demonstrated, for this active region, that the low-FIP elements are overabundant in the corona by a factor of 8.2 (−5.4, +5.0) relative to hydrogen, while the high-FIP elements other than H are overabundant in the corona by a factor of 2.3 (−5.4, +5.0). The uncertainty in our measured hydrogen abundance limits a determination of whether the abundances of the high-FIP elements (except H) are nearly the same in the photosphere and corona or are enhanced. Equivalently, this uncertainty prevents us from establishing whether hydrogen fractionates in the corona to the same degree as the other high-FIP elements. However, it is clear, in spite of the magnitude of this uncertainty, that hydrogen does not behave as a low-FIP element in the corona.

5. DISCUSSION OF ANALYSIS TECHNIQUE

Next, we consider to what extent our relative and absolute abundance measurements might be affected by various factors, including the instrumental calibration, the evolution of the region over time, and the effects of optical depth, a multithermal plasma, the assumed iron ionization balance, or the assumed line broadening. We show that these factors have no significant effect on our results. Specifically, these additional considerations do not change the measured relative elemental abundances or the conclusion that hydrogen does not fractionate as a low-FIP element in the corona.

5.1. *Instrumental Calibration*

If the relative instrumental responses of the AS&E sounding-rocket payload and the FCS were not correctly understood, we would expect to find two separate solutions of emission measure (for the same isothermal model) from the observations, one from the FCS line data and one from the broadband images.

For an isothermal plasma with Meyer's adopted coronal abundances, the emission measures from the broadband data are about 30% lower than the emission measures derived from the FCS lines at active-region temperatures. This discrepancy is within the uncertainties of the data, as indicated by the minimum reduced χ^2 values of less than unity in this range of temperatures.

For an isothermal plasma with photospheric composition, the FCS line intensities are inconsistent with one another as well as with broadband observations, indicating that problems with the relative instrumental calibration could not have the

effect of creating the apparent FIP bias in the coronal abundances.

5.2. *Evolution of the Active Region*

As discussed earlier, active region AR 4901 was observed to have brightened in the Fe XVII line at 15.01 Å: the central pixel of the last Fe XVII map, the area of interest, had about 50% more counts than the corresponding pixel of the first Fe XVII map. These two Fe XVII maps span the time of FCS observation, so this brightening could have happened at any time during this approximately 30 minute period. It seems unlikely that an increase in the intensity of the region caused the apparent FIP bias in the coronal abundances. The O VIII and Ne IX measurements were taken near the middle of the observing period, at 18:13 UT and 18:21 UT, respectively. These two lines of high-FIP elements are not consistent with the lines of low-FIP elements, for photospheric abundances. A change in the brightness of the region of the magnitude of the FIP differential (a factor of 3.5) would be apparent in the Mg XI data, which were taken simultaneously with the O VIII data, as well as in the broadband images (at 18:17 UT) taken in the time period of the O VIII (18:08–18:15 UT) and Ne IX (18:15–18:21 UT) observations. Since such a decrease is not observed in the Mg XI flux or in the broadband fluxes, the FIP-differential of the elemental abundances deduced from these data is not likely to be an effect of a change in the brightness of the active region over time.

5.3. *Optical Depth*

The optical depths of some of the lines, especially the Fe XVII line at 15.01 Å, are significant compared with the uncertainties of the flux measurements, so the effects of optical depth must be taken into consideration in the determination of the coronal abundances. If we assumed that these FCS lines were optically thin, then the observed line and broadband intensities would be inconsistent with a plasma having either set of relative abundances, at any temperature: the minimum reduced χ^2 of the intensities of an optically thin plasma is 6.2 for the adopted coronal abundances (Meyer 1985b) and is 11.6 for photospheric abundances.

The optical depth of the lines gives us the additional information needed for a diagnostic of absolute abundance. It is not possible from our temperature and emission measure models alone to determine whether the abundances of the high-FIP elements are depleted in the corona relative to the photosphere, as proposed by Meyer (1985b), or whether the abundances of the low-FIP elements are enhanced, as recent evidence suggests (Meyer 1993a, 1993b), because there is no separate measurement of the continuum in this data set from which to directly measure the abundance of hydrogen. For the adopted coronal abundances (Meyer 1985b), emission from iron lines dominates the broadband spectra at active-region temperatures, as shown by Figures 5*a* and 5*b*. The continuum contributes less than 20% of the total filtered spectrum of both of the broadband filters. Thus, if all the lines in this region actually were optically thin, then no information on absolute abundances would be present in the data.

5.4. *Broadband Temperature Map*

The temperature distribution within the 30″ × 30″ area of interest can be examined by looking at a broadband temperature map made from the ratio of the images through two different filters. Figure 9 shows a contour plot of the temperature derived from the broadband images in the area observed by the FCS collimator. (This is the area over which the line profile observations were made.) Within the area of interest, the line-of-sight temperatures (for 6″ × 6″ resolution elements) vary from 2.3×10^6 to 3.0×10^6 K. This range of temperatures corresponds to values of the minimum reduced χ^2 of near unity for the Meyer (1985b) adopted coronal abundances (Figure 7*b*). Most of the line-of-sight temperatures in this map are within the range of isothermal temperature solutions (2.5×10^6 to 3.0×10^6 K), especially considering that the pyramidal field of view of the FCS collimator weights the material at the center more heavily in the intensity measurement.

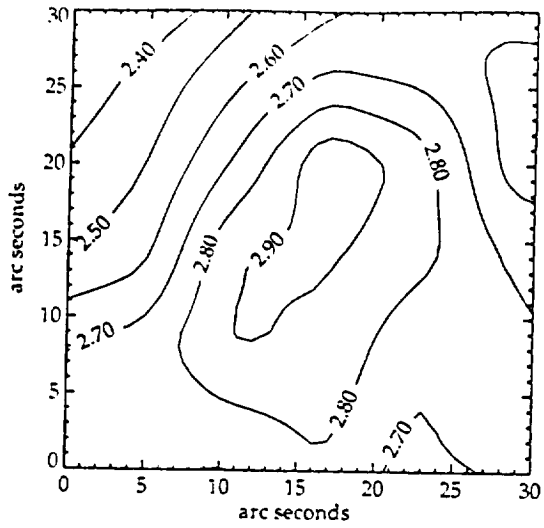

FIG. 9.—Temperature map, in units of 10^6 K, of the area of joint observation near the center of AR 4901. The temperature map is calculated from the ratio of the polypropylene-filtered and the beryllium-filtered broadband soft X-ray images, assuming that the region is isothermal along the line of sight. The adopted coronal abundances (Meyer 1985b) are used in the calculation. The line-of-sight temperatures in this region range from 2.3×10^6 K to 3.0×10^6 K.

5.5. *Multithermal Analysis*

Next we consider the effect of a multitemperature plasma on the abundance diagnostic. We will allow the active-region temperature to vary along the line of sight as well as perpendicular to it. For a nonisothermal plasma, the definition of emission measure, $\int n_e^2\, dl$, is no longer applicable. In the multithermal case, we use the differential emission measure, $\xi(T)$.

Empirically determined differential emission measures (DEMs) (e.g., Dere & Mason 1993) can be well approximated at coronal temperatures by a Gaussian shape. We assume that the DEM for this active region, $\xi(T)$, has a Gaussian shape described by three parameters—the temperature corresponding to the peak of the Gaussian curve (T_{max}), the half-width of the curve (ΔT), and a multiplicative factor (ξ_0):

$$\xi(T) = \xi_0 \exp\left[-\frac{(T - T_{max})^2}{2(\Delta T)^2}\right]. \quad (11)$$

For a differential emission measure of this form, the intensity of a coronal emission line at the Sun is given by the expression

$$F_i = P\xi_0 \int \epsilon_i(T) \exp\left[-\frac{(T - T_{max})^2}{2(\Delta T)^2}\right] dT \quad (12)$$

Similarly, the broadband flux incident on the film is given in terms of the differential emission measure by the expression

$$F_i = \frac{A}{4\pi f^2}\,\xi_0 \int \exp\left[-\frac{(T - T_{max})^2}{2(\Delta T)^2}\right] \int p(\lambda, \log T)\eta_i(\lambda)\,d\lambda\,dT\ . \tag{13}$$

The integral over temperature in equations (12) and (13) is evaluated over the entire range of formation temperatures for each line or broadband spectrum.

The value of the minimum reduced χ^2 is calculated for a range of values of the peak temperatures, T_{max} (1×10^6 K to 10×10^6 K) and half-widths, ΔT (0.1×10^6 K to 10×10^6 K). The scaling factor ξ_0 that yields the minimum reduced χ^2 for each (T_{max}, ΔT) pair is determined. If $\chi^2_0(T)$ is less than or equal to unity for any value of the DEM scaling factors, then the data are consistent with a plasma having a Gaussian DEM described by the given T_{max} and ΔT.

The values of the minimum reduced χ^2 for each pair of DEM parameters, T_{max} and ΔT, are plotted on a contour plot, in Figure 10*a* for a plasma with photospheric abundances and in Figure 10*b* for one with the adopted coronal abundances. As in the isothermal case, there is no Gaussian DEM model for which $\chi^2_0(T)$ is equal to or less than eight, indicating that the observations are not consistent with a plasma having photospheric abundances and a Gaussian DEM. For the adopted coronal abundances (Meyer 1985b), shown in Figure 10*b*, there are a range of DEMs for which the $\chi^2_0(T)$ is less than or equal to unity. This indicates that the data are consistent with multithermal plasmas having the adopted coronal relative abundances (Meyer 1985b) and a range of Gaussian DEMs.

The dotted lines plotted over the contours in Figure 10*b* show the isothermal plasma temperatures that are consistent with the data. For narrower Gaussian DEMs, the range of peak temperatures that are consistent with the data approaches the range of isothermal temperatures solutions. Plasmas having Gaussian DEMs with half-widths of up to 6×10^5 K are consistent with the data for peak temperatures near to or lower than the temperatures of the isothermal solutions. It is not possible to distinguish between the multithermal models and the isothermal models on the basis of these data—any plasma model that fits the data satisfactorily (i.e., has a minimum reduced χ^2 of one or less) is a possible solution for the plasma properties of the region.

We have shown that there are multithermal DEM models as well as isothermal models that are consistent with the observations for plasmas with Meyer's (1985b) adopted coronal relative abundances, but not for those with photospheric abundances. Therefore, it is not likely that the apparent depletion of the high-FIP abundances relative to the low-FIP abundances in the corona is an effect of a multithermal temperature distribution.

5.6. *Iron Ionization Fractions*

The ionization balance calculations used in this paper are those of Arnaud & Rothenflug (1985). Recently, the ionization equilibrium of iron has been recalled by Arnaud & Raymond (1992). Saba & Strong (1992) have found difficulties in the interpretation of FCS data with these new iron ionization fractions. Since we have measurements of only three iron lines (two Fe XVII lines and one Fe XVIII line), it is not possible, given the uncertainties in the measured fluxes of these lines, to determine which of these iron ionization balance calculations is more accurate. In our analysis, we chose to use the Arnaud & Rothenflug (1985) ionization fractions for consistency, as they are assumed in the emissivities (Mewe et al. 1985) used in the interpretation of the broadband spectra. In this section we discuss how the assumption of the Arnaud & Raymond (1992) iron ionization fractions would affect our results.

5.6.1. *Relative Abundances*

The relative abundance results are the same for the assumption of either iron ionization balance—the observations are not consistent with an isothermal plasma of photospheric abundances, but are consistent with an isothermal plasma with the adopted coronal abundances of Meyer (1985b) for a range of temperatures from 2.6×10^6 K to 3.0×10^6 K.

5.6.2. *Absolute Abundances*

The absolute abundance calculation is affected by the choice of iron ionization fractions, but the result that hydrogen does not behave as a low-FIP element in the corona is not changed.

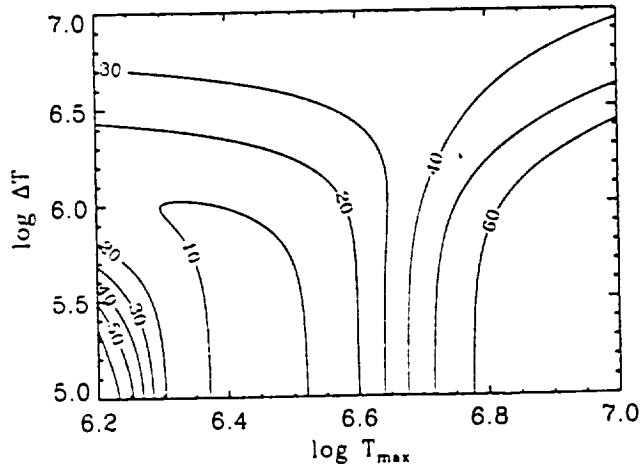

FIG. 10*a*

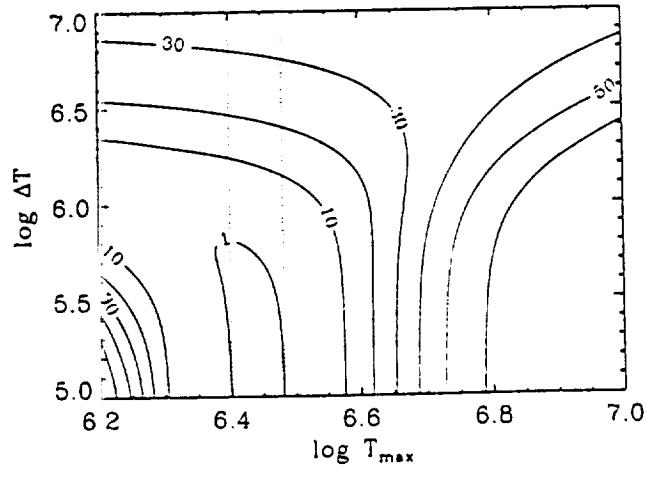

FIG. 10*b*

FIG. 10.—Contour maps of minimum reduced χ^2, showing the fit of Gaussian DEM models to the data as a function of T_{max} and ΔT for (*a*) the photospheric abundances and for (*b*) the adopted coronal abundances (Meyer 1985b).

For the Arnaud & Raymond (1992) values, the path length is about 50% longer than the path length calculated in § 4.2. This leads to an iron abundance relative to hydrogen of 7.4×10^{-4} (-4.9×10^{-4}, $+4.6 \times 10^{-4}$), meaning that the low-FIP elements must be overabundant in the corona by a factor between 6 and 31.

5.7. *Nonthermal Velocities*

The statistics of these FCS line profile data do not allow us to accurately measure the excess line broadening. Therefore, for this analysis, a value of the nonthermal velocity was assumed based on other coronal observations. Measurements of nonthermal broadening of coronal active-region lines vary from 10–30 km s^{-1} (Cheng, Doschek, & Feldman 1979) from cooler EUV lines, to 26 ± 5 km s^{-1} from a 1.3×10^6 K Mg line (Hassler et al. 1990), to 44 km s^{-1} for the average of a 3×10^6 K active region (with a range 0–60 km s^{-1} over the active region) from the Mg XI line at 9.17 Å (Saba & Strong 1991).

We arbitrarily assumed 20 km s^{-1} as an intermediate value of nonthermal velocity and then investigated the effects of assuming nonthermal velocities ranging from 0 km s^{-1} to 60 km s^{-1} on our abundance results. The nonthermal velocities of all the FCS lines were assumed to be same, although only the nonthermal velocity assumed for the Fe XVII line at 15.01 Å has a significant effect on our results.

The relative abundances determined from these observations are unchanged for the assumption of any nonthermal velocity in this range.

The effect of the nonthermal velocity assumption on the absolute abundance of iron relative to hydrogen derived from observations of this active region is dependent on the magnitude of the excess velocity relative to the Fe XVII (15.01 Å) thermal velocity of 29 km s^{-1}: if we assumed that the lines were thermally broadened only (as Schmelz et al. 1992 did for these same FCS observations), then the derived absolute abundance of iron would decrease by only 20% from the value obtained in § 4.2.2 for $v_{nt} = 20$ km s^{-1}. For a nonthermal velocity of 29 km s^{-1}, the derived absolute abundance of iron is 30% greater than it is for $v_{nt} = 20$ km s^{-1}. However, the absolute abundance of iron determined from these observations is significantly increased over our previous result of § 4.2.2 if nonthermal velocities larger than 29 km s^{-1} are assumed: for $v_{nt} = 40$ km s^{-1} the absolute abundance of iron is increased by a factor of 2, and for $v_{nt} = 60$ km s^{-1} the absolute abundance of iron is increased by a factor of 3.7. Qualitatively, the effect of the assumed nonthermal broadening on this analysis does not change the conclusion that the abundance of iron is enhanced in the corona relative to hydrogen and that, therefore, hydrogen behaves more as a high-FIP element than as a low-FIP element in the corona. Qualitatively, the degree of iron enhancement in the corona is significantly greater for the assumption of nonthermal contributions to the line widths of greater than 30 km s^{-1}.

6. SUMMARY

The simultaneous broadband and line intensity data from the center of the observed coronal active region confirm the FIP separation of Meyer's (1985b) adopted coronal abundances of O, Ne, Mg, and Fe and put these abundances on an absolute scale with respect to hydrogen. The low-FIP heavy elements are found to be overabundant in this coronal active region by a factor of 3.5 relative to the high-FIP elements. We find that hydrogen behaves more like a high-FIP element in the corona, as suggested by Meyer (1993a, 1993b) and Feldman (1992), than like a low-FIP element (Meyer 1985b): in this coronal active region, hydrogen is a factor of 8.2 (-5.4, $+5.0$) less abundant relative to the heavy elements than in the photosphere.

The systematic uncertainties in this analysis arise primarily from the assumptions of the ionization fraction, the density structure of the active region, and the nonthermal line broadening. These uncertainties do not change our relative abundance results, but they all tend to increase our derived absolute abundance of iron. Considering the systematic and statistical uncertainties we conclude that the abundance of hydrogen relative to iron must be depleted in the corona compared to the photosphere by a factor of at least 2.3 in this active region, but it may be depleted by more than an order of magnitude more. Even in the most extreme case, the systematic uncertainties do not affect the conclusions that, for this active region, hydrogen does not fractionate as a low-FIP element in the corona and the relative abundances of O, Ne, Mg, and Fe conform to the FIP-separation discussed in the review by Meyer (1985b).

This paper is based on the Ph.D. thesis of K. W., whose graduate work was supported by NASA Graduate Student Researchers Program grant NGT-50308. Part of this work was done while K. W. held a National Research Council—Naval Research Laboratory Research Associateship. The acquisition and comparison of the *SMM* XRP data and the AS&E broadband data were supported by the *SMM* Guest Investigator Program under contract NAS 5-30141. The broadband data were obtained by the AS&E Sounding-Rocket Program under contracts NAS 5-25496 and NAS 5-31619. D. M. has also been supported at NRL in this work by NASA under contract NDPR H-06877D and by the Office of Naval Research. J. L. R. S. and K. T. S. were supported by NASA contracts NAS 5-28713 and NAS 5-30431 and by the Lockheed Independent Research Program, D. F. W. by the Air Force Phillips Laboratory GPS under AF19628-87-K-0033 and AF19628-90-K-0006 and by NASA under NAS 5-30141, and D. M. Z. by NASA contracts NAS 5-28713 and NAS 5-30431. The synthetic soft X-ray solar spectra used in the analysis of the broadband images were generated by a program provided by J. R. Lemen of Lockheed Solar and Astrophysics Laboratory.

K. W. thanks J. F. C. Wardle, S. F. Kahler, D. Roberts, J. W. Cook, P. A. Lund, and K. G. Widing for extensive discussions. We also appreciate help and comments from G. E. Brueckner, J. Brosius, J. M. Davis, J.-P. Delaboudiniere, G. A. Doschek, J. Gurman, S. Habbal, G. Holman, J.-P. Meyer, and J. Raymond. For extensive technical support, we thank M. Purington, R. Schueller, the AS&E sounding rocket instrument team, and the XRP instrument team.

K. W. is greateful to American Science and Engineering Inc., for its hospitality and support.

REFERENCES

Abu-Salbi, N., & Callaway, J. 1981, Phys. Rev. A, 24, 2372
Acton, L. W. 1978, ApJ, 225, 1069
Acton, L. W., et al. 1980, Solar Phys., 65, 53
Arnaud, M., & Raymond, J. 1992, ApJ, 298, 394
Arnaud, M., & Rothenflug, R. 1985, A&AS, 60, 425
Bevington, P. R. 1969, Data Reduction and Error Analysis for the Physical Sciences (New York: McGraw-Hill), 313
Bhatia, A. K., & Doschek, G. A. 1992, Atomic Data Nucl. Data, 52, 1
Brenneman, H. H., & Stone, E. C. 1985, ApJ, 299, L57
Cheng, C.-C., Doschek, G. A., & Feldman, U. 1979, ApJ, 227, 1037
Cook, J. W., Ewing, J. A., & Sutton, C. S. 1987, PASP, 100, 402
Cornille, M., Dubau, J., Loulergue, M., Bely-Dubau, F., & Faucher, P. 1992, A&A, 259, 669
Dere, K. P. 1982, Solar Phys., 77, 77
Dere, K. P., & Mason, H. E. 1993, Solar Phys., 144, 217
Fawcett, B. C. 1984, Atomic Data Nucl. Data, 31, 495
Feldman, U. 1992, Phys. Scripta, 46, 202
Geiss, J. 1982, Space Sci. Rev., 33, 201
Grevesse, N., & Anders, E. 1991, in Solar Interior and Atmosphere, ed. A. N. Cox, W. C. Livingston, & M. S. Matthews (Tucson: Univ. Arizona Press), 1227
Grevesse, N., Noels, A., & Sauval, A. J. 1992, in Proc. 1st SOHO Workshop (ESA SP-348) (Noordwijk: ESA Publications Division, ESTEC), 305
Hagelstein, P. L., & Jung, R. K. 1987, Atomic Data Nucl. Data, 37, 121
Hassler, D. M., Rottman, G. J., Shoub, E. C., & Holzer, T. E. 1990, ApJ, 348, L77
Kato, T., & Nagazaki, S. 1989, Atomic Data Nucl. Data, 42, 313
Lemen, J. R. 1990, private communication
Mewe, R., Gronenschild, E. H. B. M., & van den Oord, G. H. J. 1985, A&A, 62, 197
Meyer, J. P. 1985a, ApJS, 57, 151
———. 1985b, ApJS, 57, 173
Meyer, J. P. 1993a, Adv. Space Res., 13, 377
———. 1993b, in Origin and Evolution of the Elements, ed. N. Prantzos, E. Vangioni-Flam, & M. Cassé (Cambridge Univ. Press), 26
Moses, J. D., Krieger, A. S., & Davis, J. M. 1986, Proc. SPIE, 691, 138
Moses, J. D., Schueler, R., Waljeski, K., & Davis, J. M. 1989, Proc. SPIE, 1159, 551
Nitta, N., et al. 1991, ApJ, 374, 374
Rugge, H. R., & McKenzie, D. L. 1985, ApJ, 297, 338
Saba, J. L. R., & Strong, K. T. 1991, ApJ, 375, 789
———. 1992, Proc. 1st SOHO Workshop (ESA SP-348) (Noordwijk: ESA Publications Division, ESTEC), 347
Sampson, D. A., Zhang, H. L., & Fontes, C. J. 1991, Atomic Data Nucl. Data., 48, 25
Schmelz, J. T., Saba, J. L. R., & Strong, K. T. 1992, ApJ, 398, L115
Vaiana, G. S., Krieger, A. S., & Timothy, A. F. 1973, Solar Phys., 32, 81
Vaiana, G. S., Van Speybroeck, L., Zombeck, M. V., Krieger, A. S., Silk, J. K., & Timothy, A. 1977, Space Sci. Instr., 3, 19
Veck, N. J., & Parkinson, J. H. 1981, MNRAS, 197, 41
Waljeski, K. 1992, Properties of Solar Coronal Active Regions, Ph.D. thesis, Brandeis Univ. (Ann Arbor: University Microfilms International Dissertation Information Service)
Webb, D. F., & Davis, J. M. 1985, Solar Phys., 102, 177
Widing, K. G., & Feldman, U. 1989, 344, 1046
Wiese, W. L., Smith, M. W., & Glennon, B. M. 1966, Atomic Transition Probabilities. Vol. 1, Hydrogen through Neon (Washington, DC: NSRDS National Bureau Standards)
Wiese, W. L., Smith, M. W., & Miles, B. M. 1969, Atomic Transition Probabilities. Vol. 2, Sodium through Calcium (Washington, DC: NSRDS National Bureau of Standards)
Zhang, H. L., & Sampson, D. H. 1987, ApJS, 63, 487
———. 1989, Atomic Data Nucl. Data, 43, 1